Phylogeny of SK channels and functional characterization of the conserved Phe in the S3–S4 loop

Short title : Conserved S3–S4 Phe in SK channels

Antoine Mouchet,[1] Valerian Lupo,[2,3] Alexandre Grignard,[1] Théo Nadenoen,[1] Romain Vitello,[4] Alain Brans,[1] Vincent Seutin,[5] Jean-François Liégeois,[4] Frédéric Kerff [1*]

1 InBioS- Centre for Protein Engineering, Laboratory of Crystallography, University of Liège, 4000 Liège, Belgium
2 InBioS–PhytoSYSTEMS, Eukaryotic Phylogenomics, University of Liège, 4000 Liège, Belgium
3 BCCM/MUCL and Laboratory of Mycology, Earth and Life Institute, Université Catholique de Louvain, 1348 Louvain-la-Neuve, Belgium
4 Laboratory of Medicinal Chemistry, CIRM, University of Liège, 4000 Liège, Belgium
5 Laboratory of Neurophysiology, GIGA, University of Liège, 4000 Liège, Belgium

*fkerff@uliege.be

Abstract

Small conductance calcium-activated potassium channels ($K_{Ca}2.x$ or SK) are critical regulators of neuronal excitability, and dysregulation of their function is linked to central nervous system disorders, including schizophrenia and depression. Structural analyses of the SK2 channel identified a phenylalanine at the tip of the S3–S4 extracellular loop as a key determinant for channel blockade by apamin and UCL1684. To investigate the functional significance of this residue, we used site-directed mutagenesis to substitute phenylalanine with either alanine or tyrosine in both SK2 and SK3 subtypes. Electrophysiological recordings and ligand binding assays revealed that the alanine substitution render both channels insensitive to the two compounds. The phenylalanine-to-tyrosine substitution has no significant impact on the sensitivity of SK channels to UCL1684, indicating a conserved conformation of the S3-S4 loop and the specific low conductance structure of the selectivity filter. The SK3 tyrosine mutant does however display a fivefold reduced sensitivity to apamin possibly linked to an additional stabilizing H-bond between the tyrosine and the selectivity filter. The tyrosine mutation is not expected to significantly affect K^+ current according to molecular dynamic simulations.

The phylogeny of SK channels (SK1-4) is consistent with a model of vertebrate gene evolution driven by a whole-genome tetraploidization, with the first duplication occurring prior to the last common ancestor of vertebrates, and the second occurring separately after the split between jawless fishes and jawed vertebrates lineages. SK4 channels form a divergent group of paralogs presenting an early loss of the SK characteristic S3-S4 loop. A tyrosine residue represents the most frequent natural substitution of the conserved S3-S4 phenylalanine and most occurrences are found in a predominantly monophyletic group within the SK2 channel branch. Natural selection may have promoted this substitution by conferring reduced sensitivity to peptidic toxins produced by competing species, as illustrated by the human SK3–apamin interaction.

Statement of significance

Small conductance calcium-activated potassium (SK) channels regulate neuronal excitability and are implicated in neuropsychiatric disorders. A conserved phenylalanine within the S3–S4 extracellular loop is a critical determinant of small conductance and channel sensitivity to the apamin and UCL1684 blockers in SK2 and SK3 subtypes. Mutational analysis reveals that substitution of this residue with alanine abolishes inhibitor sensitivity, while

tyrosine substitution selectively reduces apamin sensitivity of SK3 likely without disrupting K^+ conductance. Phylogenetic analysis indicates that this residue has been mostly conserved throughout evolution but was lost early in the SK4 group. These findings link SK channel pharmacology, structural determinants of pore function, and evolutionary adaptation, providing new insights into how extracellular loop architecture shapes K^+ channel regulation and toxin sensitivity.

Introduction

Small conductance calcium-activated potassium channels ($K_{Ca}2.x$ or SK) are selective for K^+ ions and their opening depends upon the Ca^{2+} concentration in the cytoplasm (1–3). Calcium ions bind calmodulin molecules which form a complex with SK proteins and thereby allow the opening of the channel through conformational changes (4). Three subtypes of SK proteins (SK1-3, encoded by *KCNN1-3*) have been cloned (5) and shown to be expressed in various tissues and organs in mammals (e.g. nervous system, pancreatic islet cells, atrial and endothelial cells) (6–10), displaying differential expression throughout the central nervous system (CNS). In situ hybridization and immunohistochemistry experiments in the rat revealed that SK1 and SK2 subtypes show overlapping expression in regions including the neocortex and hippocampus while SK3 expression is more prominent in subcortical areas (e.g. thalamus and monoaminergic cell regions) (11).

In the CNS, SK channels play an essential role in regulating excitability by mediating the medium duration afterhyperpolarization (mAHP). Thus, blocking SK channels enhances excitability while increasing their opening decreases excitability (12–14). In consequence, SK channel modulation represents a promising strategy in the fight against various disorders of the CNS such as ataxia (15), schizophrenia (16) or mood disorders (17), the latter being supported by a mouse model with chronic social isolation-induced anxiety/depressive-like behaviors, in which serotonergic neuron excitability is decreased by an upregulation of SK3 channel function. The presence of different subtypes of SK channels (notably SK2 in humans) in cardiomyocytes indicates that they could also represent interesting targets for the treatment of atrial fibrillation (18,19).

Several molecules are capable of blocking SK channel activity, but they are hardly usable for therapeutic purposes due to a lack of subtype-selectivity or a narrow therapeutic window. Apamin, a 18 amino acids peptide extracted from bee venom, is the archetypal inhibitor used for the study of SK channel structure and functions (1). It exhibits exceptionally high binding affinity towards all three SK channel subtypes, with affinity constants (K_D) in the low picomolar range (~ 4 – 10 pM) for SK2 and SK3, and around 300 pM for the human SK1 isoform (20–22). However, apamin displays a differential block for each of them with human SK2 being more sensitive (IC_{50} values from 27 to 140 pM) than SK3 (0,63 to 4 nM) and SK1 currents (0,7 to 12 nM) (23,24). This suggests a critical step, which may be different in SK2 and SK3, between binding and block. UCL1684, a bisquaternary molecule permanently charged which acts on the same binding site as apamin, is also a blocker of SK channel activity

but its selectivity for the different subtypes is low, as indicated by the IC_{50} values (~750 pM, ~350 pM and from 2.5 to 9.5 nM for SK1, 2 and 3 respectively) (25,26). Finally, tetraethylammonium (TEA), a charged quaternary ammonium salt, is a nonspecific blocker of potassium channels. It has been shown to inhibit a broad range of K^+ channels, including voltage-dependent and calcium-activated K^+ channels, by acting as a plug on top of the selectivity filter (20). Different studies revealed that TEA blocks SK2 and SK3 channels with an IC_{50} value of approximately 5-10 mM (20,27). Other compounds such as AG525E1 or NS8593 have also been shown to reduce SK activity but they also display poor selectivity in blocking SK channel subtypes (9,28).

Numerous mutagenesis studies have been conducted to elucidate the molecular mechanism underlying apamin's action, identifying key amino acid residues that influence its binding and inhibitory effects. Notably, several residues located in the extracellular vestibule of the pore, including a histidine conserved in both SK2 and SK3 subtypes, were found to be critical for effective interaction and subsequent channel blockade by the toxin (20,29). Within the pore region, a conserved valine present in SK2 and SK3 also appears to contribute significantly to apamin and TEA sensitivity (27). Furthermore, two independent studies highlighted the regulatory role of three residues within the S3–S4 extracellular loop, suggesting that this segment strongly modulates apamin affinity and channel inhibition (25,30). The functional significance of the S3–S4 loop was substantiated by AlphaFold2 models and further refined by the recent determination of the SK2 channel's 3D structure via cryo-electron microscopy studies that include complexes with some SK modulators including UCL1684 and apamin (31–33). Structural analyses revealed that the S3–S4 loop adopts a β-hairpin shape, with each of the four channel subunits contributing to a canopy-like formation that overlays the pore domain. At the tip of this loop—right at the exit of the channel pore and near the selectivity filter—a phenylalanine residue was shown to be essential for both the proper folding of the loop and the binding of apamin and UCL1684. Several residues within the loop, including the phenylalanine, directly interact with the selectivity filter, inducing conformational changes that contribute to the low unitary conductance characteristic of SK channels (31).

Building on prior structural characterizations of SK2 and a thorough phylogeny of SK channels that includes the intermediate conductance K^+ channel SK4 (IK/K_{Ca}3.1), this study focuses on the functional and structural relevance of the S3–S4 β-hairpin loop and the conserved phenylalanine located at its tip. Using site-directed mutagenesis, this phenylalanine was substituted with either alanine or tyrosine in both SK2 and SK3 subtypes. *In vitro* binding

assays, in combination with electrophysiological recordings, confirm the essential role of this residue in mediating high-affinity interactions with the channel blockers UCL1684 and apamin.

Materials and methods

DNA construct, cell culture and preparation of biological material

Wild-type human SK2 (NM_021614.3) and SK3 (NM_002249.6) genes, cloned in the pcDNA3.1-c-(k)DYK vector, were obtained from GenScript (catalog numbers OHu21556D and OHu22129D, respectively). Point mutations were generated via PCR using the Q5® Site-Directed Mutagenesis kit from New England Biolabs (Ipswich, Massachusetts, USA) and were verified by DNA sequencing. Channels were transiently expressed in HEK293 cells. For each passage, cells were dissociated using a Trypsin-EDTA solution (Gibco©) and maintained in Dulbecco's Modified Eagle Medium (DMEM) with high glucose and stable-glutamine (Biowest©), supplemented with 10% Fetal Bovine Serum (Sigma-Aldrich©) and a Penicillin-Streptomycin mix (Invitrogen©), at 37°C in a 5% CO_2 atmosphere.

For electrophysiology experiments, cells were plated in 35 mm Petri dishes (Falcon©) and co-transfected with EGFP-containing plasmids and SK plasmids 24 hours later. First, the complete DMEM medium was replaced with serum-free DMEM. Then, a mixture consisting of 50 µL of 0.2 µg/µL polyethyleneimine (M.W. 25000 Da, Alfa Aesar©), 10 µL of 0.1 µg/µL GFP plasmids, 15 µL of 0.1 µg/µL SK plasmids, and 125 µL serum-free DMEM, pre-incubated for 20 minutes, was added to the medium. Cells were used for patch-clamp experiments 16 to 24 hours post-transfection.

For membrane preparation, HEK293 cells were plated on 100 mm Petri dishes for 24 to 48 hours until reaching approximately 90% confluence. They were then transfected with the corresponding plasmid in a 0.2 µg/µL polyethyleneimine solution. Cells were harvested 48 hours later by trypsinization at 37°C and concentrated by centrifugation at approximately 250 x g for 5 minutes at room temperature. Cells were resuspended in cold PBS (4°C) using 3 mL per dish and centrifuged twice for 10 minutes at 1000 x g (4°C). The pellet was resuspended in a lysis buffer (50 mM Tris, 1% BSA, pH 7.4) using 1 mL per dish, mixed thoroughly using a 21G needle mounted on a syringe, and centrifuged for 10 minutes at 200 x g (4°C). The supernatant was then centrifuged for 25 minutes at 20000 x g (4°C), and the pellet was resuspended in a storage buffer (50 mM Tris, 5 mM KCl, pH 8.5) before being centrifuged again for 25 minutes at 20000 x g. The final pellet was resuspended in the same buffer using 1 mL per dish. Protein concentration was determined using a colorimetric protein assay with a

bicinchoninic acid kit (Pierce), and the absorbance was measured at 560 nm with a FlexStation 3 (Molecular Devices) spectrophotometer. Glycerol (10%) was added, and aliquots were stored at -80°C.

[^{125}I]-Apamin binding

Binding assays were performed in a 10 mM Tris-HCl buffer (pH 7.5) containing 0.1% BSA and 5mM KCl. The radioligand ^{125}I-apamin, with a specific activity of 2000 – 2200 Ci / mmol was obtained from PerkinElmer. Unlabeled apamin was diluted in mQ water at a concentration of 400 µM as stock solution and aliquots were stored at -20°C before use. Glass fiber filters (Whatman GF/C, Maidstone, Kent, UK) used in these experiments were coated for 1h in 0.5% polyethyleneimine to prevent apamin from binding to the filter, then washed with 2.5 ml of ice-cold buffer just before use. For the screening of the different mutant channels, 950µL of membrane preparations (final protein concentration: 10 µg/ml) were incubated for 1h at 0°C with 25µL of 5pM ^{125}I-apamin in presence of 25µl of 0.1µM mQ water to measure the "Total" binding or in presence of 25µL of 0.1µM unlabeled apamin for the "Non-specific" binding. The protocol was the same for the saturation assay on the SK2 tyrosine mutant except that a range of radiolabeled apamin concentrations from 1 pM to 200 pM was used. At the end of the incubation period, aliquots were filtered under reduced pressure through Whatman filters. Filters were rapidly washed twice with 2.5 ml of ice-cold buffer and placed into a vial containing 7.5ml of scintillation liquid. Radioactivity was evaluated with a Packard Tri-Carb 2300TR Beta-counter after a minimum of 3 hours of contact in absence of light.

Electrophysiology

Petri dishes containing HEK293 cells were placed into a recording chamber and superfused at room temperature with an external control solution containing 120 mM KCl, 1.44 mM $MgCl_2$, 10 mM glucose, 10 mM HEPES, 6.19 mM $CaCl_2$, and 10 mM EGTA, with the pH adjusted to 7.4 using 10 mM KOH. The pipettes, made from borosilicate glass (code 1403513, Hilgenberg, Malsfeld, Germany), were pulled so that the tip of the pipettes was 1-2 µm and the access resistance generally ranged from 2 to 5 MΩ. Pipettes were filled with an internal solution consisting of 120 mM KCl, 2.34 mM $MgCl_2$, 9.95 mM $CaCl_2$ (10 µM free Ca^{2+}), 10 mM EGTA, 10 mM HEPES, and 1.5 mM Na_2ATP, adjusted to pH 7.4 with 10 mM KOH. SK currents were recorded using the whole-cell configuration under symmetrical high potassium conditions, applying voltage ramps from -80 to +80 mV in 1 second (ramp speed = 160 mV/s). Currents were recorded using a MultiClamp™ 700B Microelectrode amplifier (Axon Instruments) and

filtered at 10 kHz using a low pass Bessel filter. Sampling frequency was 10 kHz. We did not attempt to correct for series resistance errors because in our experience these errors would not alter the measurement of the potency of the compounds to block the channels.

Apamin and UCL1684, sourced from Tocris Biosciences (Bristol, UK), were prepared as stock solutions in water and DMSO respectively, each at a concentration of 300 µM, and stored at -20°C. The experimental solutions were prepared on the day of the experiment by diluting these stock solutions with the external solution. Control experiments showed that 0.1 % DMSO (the maximal concentration used) had by itself no effect on SK currents. Tetraethylammonium (TEA, obtained from Sigma) solutions were also prepared freshly on the day of the experiment by dissolving the powder directly into the external solution.

Data analysis and statistics

Data analysis was carried out using GraphPad Prism 10.5.0 (GraphPad Software, San Diego, CA). For saturation binding experiments, data were fitted with equation Eq. 1:

$$Y = B_{max}\frac{X}{(X+K_D)} \qquad \text{Eq. 1}$$

with X being the concentration of radioligand, Y the specific binding, B_{max} the maximum binding and K_D the dissociation constant of the ligand.

For the electrophysiological experiments, concentration-response curves were fitted using the variable slope Hill equation Eq. 2:

$$Y = Bottom + \frac{(Top-Bottom)}{(1+(\frac{IC50}{X})^h)} \qquad \text{Eq. 2}$$

where X is the concentration of the blocker, Y is the normalized current amplitude, *Top* and *Bottom* are the plateaus, IC_{50} is the concentration of blocker that blocks 50% of sensitive current, and h is the Hill coefficient (expressed as negative values, but its absolute value is used in the text). All numerical values are expressed as mean ± S.E.M. Statistical analyses were performed using non-parametric tests (Kruskal-Wallis and Mann-Whitney).

Phylogenetic Inference

The multiple sequence alignment generated by AlphaFold3 to predict the SK3 structure was used to extract two sets of sequences with either a phenylalanine (SK-F) or a tyrosine (SK-Y) at the position corresponding to the phenylalanine of the S3-S4 loop. Each set was realigned individually using MAFFT L-INS-i v7.526 (34). The SK-Y alignment was subsequently aligned onto the SK-F alignment using Two-Scalp v243240 (A. Bertrand, V. Lupo and D. Baurain; https://metacpan.org/dist/Bio-MUST-Apps-TwoScalp) with default parameters. Conserved

sites were then selected using *ali2phylip.pl* v0.252040 (D. Baurain; https://metacpan.org/dist/Bio-MUST-Core) with the 'min' and the 'max' option set to 0.3 and 0.5, respectively. From the resulting matrix of 1,091 sequences x 389 amino acids, a first guide tree was computed using IQ-TREE v2.4.0 (35), using 1,000 ultrafast bootstrap (UFBoot) replicates (36), the 'bnni' option enabled, and ModelFinder (-m MFP option) for model selection, which identified the VT+F+R8 as the best-fit model. This guide tree was used to remove non-orthologous sequences from the alignment.

The pruned alignment was further enriched as follows. First, it was uploaded to the HMMER webserver (37), and an *hmmsearch* was performed against the "Reference Proteomes (2025_01)" database with default parameters. Results were then filtered to retain only Metazoa hits with an E-value ≤ 1e-50. The newly identified sequences were deduplicated at species level using CD-HIT v4.8.1 (38) with sequence identity threshold set to 1 and, realigned to the pruned alignment using Two-Scalp v243240 with the 'keep-length' and 'long' options enabled. Finally, low-similarity segments from some sequences in the alignment were removed using HmmCleaner.pl v243280 (39) with the `large` option enabled.

Conserved sites in the final alignment were selected using *ali2phylip.pl* v0.252040 with the 'max' and 'min' options set to 0.3 and 0.5 respectively. The resulting matrix of 4,418 sequences x 393 amino acids was used to infer a phylogenetic tree with IQ-TREE v2.4.0, under the Q.insect+R10 model (selected by ModelFinder), with 1,000 UFBoot replicates and the 'bnni' option enabled.

Publicly available dataset and detailed command line log file can be found at https://doi.org/10.6084/m9.figshare.31231342.

Structural models of SK2 and SK3

Models of SK2 and SK3 used for structural analysis and molecular dynamic simulations were generated using a locally installed version of AlphaFold3 (40). The two sequences were retrieved from the UniProt database (KCNN2 HUMAN: Q9H2S1 and KCNN3 HUMAN: Q9UGI6). Each model included four SK monomers (only folded region, residues 114-479 for SK2 and 263-628 for SK3), four molecules of human calmodulin (CALM1 HUMAN: P0DP23) 8 calcium ions (2 per N-terminal calmodulin domain) and 3 potassium ions. The structures of the human wild type SK3, SK2 F243Y (equivalent to F244 in the rat protein used for cryo-EM structures) and SK3 F392Y mutant channels were predicted using the SK2 structure (pdb_00008v2g) as unique template. For the SK2 F243A and SK3 F392A mutant, because an

effect similar to the serine mutation is expected, the SK2 F243S structure (pdb_00009eio) was used as unique template.

Docking of TEA

The docking of TEA was done on the SK2 WT (pdb_00008v2g) and SK2 F244S (pdb_00009eio) structures using the AutoDock Vina (41,42) algorithm as implemented in YASARA simulation software (43). TEA structure was imported from PubChem (PubChem CID 6285). To avoid steric hindrance and potential charge repulsion, water molecules and the two potassium ions closest to the outer pore were removed from the models. The docking simulation cell was a 20Å cube centered on the selectivity filter exit and the S3-S4 phenylalanine residue. The entire channel was considered rigid. 100 runs were done and poses with RMSD lower than 5Å were clustered together and further analyzed for binding energy.

Molecular Dynamics Simulations

The protonation states of titratable residues of all structures and models of SK2 and SK3 were determined using the H++ server (http://biophysics.cs.vt.edu/) (44). The SK2 and SK3 models were inserted into a lipid bilayer consisting of POPC, POPE, POPS, and cholesterol in a molecular ratio of 25:5:5:1, surrounded with TIP3P water molecules and K^+ and Cl^- ions, corresponding to a salt concentration of ~300 mM. The size of the simulation cells were 171.34 Å × 171.34 Å × 134.0 Å for SK2 and 173.91 Å × 173.91 Å × 130.9 Å for SK3. This setup was generated with the CHARMM-GUI Membrane Builder webserver using the ff14SB and Lipid21 force fields for proteins and lipids, respectively (45). The total number of atoms in the systems were 372165 for SK2 WT, 372155 for SK2 F243Y, 367499 for SK2 F243A, 371076 for SK3 WT, 373542 for SK3 F130Y and 371359 for SK3 F130A. Molecular dynamics (MD) simulations were run using GROMACS 2025.3 (46).

Initial energy minimization was performed using the steepest descent algorithm until the maximum force on any atom was below 1000 $kJ \cdot mol^{-1} \cdot nm^{-1}$. The minimization was run for up to 20,000 steps, with bond constraints applied to all bonds involving hydrogens. Long-range electrostatics were calculated using the particle mesh Ewald (PME) method with a 9 Å cutoff. Energy and pressure dispersion corrections were applied. During minimization, harmonic position restraints were applied with force constants of 4000, 2000, and 1000 $kJ \cdot mol^{-1} \cdot nm^{-2}$ to protein backbone, sidechain, and lipid atoms, respectively, and dihedral restraints of 1000 $kJ \cdot mol^{-1} \cdot rad^{-2}$ were included to maintain proper torsional geometry.

The system was then equilibrated in several successive MD stages under constant temperature and pressure, gradually reducing the positional and dihedral restraints to allow full relaxation. Equilibration was first performed with a 1 fs time step, using the v-rescale thermostat to maintain 303 K with separate coupling groups for the solute, membrane, and solvent. Subsequent stages employed the C-rescale barostat in semi-isotropic mode at 1 bar (τ_p = 5 ps, compressibility = 4.5×10^{-5} bar^{-1}) and progressively weaker restraints (from 4000 to 50 $kJ \cdot mol^{-1} \cdot nm^{-2}$ on backbone atoms). The integration time step was increased to 2 fs in the final stages, and all bonds involving hydrogens were constrained with the LINCS algorithm. The total equilibration time was approximately 2 ns, after which all restraints were released for the production simulation.

All MD simulations were performed with the GROMACS MD engine using the parameters shown below. Simulations used the leap-frog MD integrator with a 2.0 fs time step, for a total of 1.0 μs per simulation. Hydrogen bond lengths were constrained with the LINCS algorithm. Position-restraint were applied to residues Val390, Val391 and Ala392 with a force value of 21000 $kJ \cdot mol^{-1} \cdot nm^{-2}$ on the backbone to prevent the inner gate from closing. Temperature was controlled using the stochastic velocity-rescale thermostat separate coupling groups for solute, membrane and solvent at 303 K; the coupling time constant was 1.0 ps for all groups. Pressure was maintained at 1.0 bar with the C-rescale barostat in semi-isotropic mode using τ_p = 5.0 ps and compressibility of 4.5×10^{-5} bar^{-1} in the lateral and normal directions. Long-range electrostatics were calculated using the particle mesh Ewald (PME) method (47) with a 9 Å cutoff. The Verlet cutoff scheme was used with a neighbor list update every 20 steps. Long-range dispersion corrections for energy and pressure were applied. A uniform external electric field of 0.09 $V \cdot nm^{-1}$ was applied along the +z axis to mimic a ~400 mV transmembrane potential. MDAnalysis tools were employed for trajectory analysis of the MD simulations (48).

Results

Phylogenetic analysis of SK channels reveals naturally occurring SK channels with a tyrosine at the tip of the S3-S4 loop

Given the functional importance of the phenylalanine residue at the tip of the S3-S4 loop, we analyzed its conservation across species. A homology search based on primary structure similarity identified 4,418 sequences (see Materials and Methods), of which 780 belong to protostomes and 3,638 to deuterostomes. The resulting phylogenetic tree (Fig. 1),

rooted on Protostomia, reveals that protostomes and basal deuterostome organisms (i.e., Hemichordata, Echinodermata, Branchiostoma, and Ascidiacea) harbor a single copy of SK channel, whereas vertebrates generally possess four copies, when terminal duplication events or isoforms (e.g., alternative splicing) are not considered. Two exceptions are observed in Cyclostomata (jawless fishes), which display two copies, and Chondrichthyes (cartilaginous fishes), in which three copies were recovered in our dataset. In vertebrates, three out of the four paralogs correspond to the small-conductance calcium-activated channels SK1-SK3, whereas the fourth corresponds to the intermediate conductance channel $K_{Ca}3.1$ (SK4/IK).

We examined the distribution of amino acids at the position homologous to the phenylalanine residue located at the tip of the S3-S4 loop across the multiple sequence alignment. In protostomes, around 81.6% of the organisms (239/293) have either a missing or ambiguous (poorly aligned position) state at this position (Fig. 1 and Materials and methods), 5.5% (16/293) encode Asn, whereas the remaining organisms display other amino acids or possess multiple SK copies with mixed states, including combination of ambiguous and non-ambiguous residues. In basal deuterostomes, the phenylalanine is the most frequently observed amino acid. Specifically, 100% of organisms from Branchiostoma and Ascidiacea lineages display a phenylalanine at this position, whereas the single Hemichordata organism carries a tyrosine; in Echinodermata, 62.5% (5/8) and 37.5% (3/8) of organisms exhibit phenylalanine and tyrosine residues, respectively.

In vertebrates, phenylalanine remains the predominant residue at this position, both in the two paralogs of Cyclostomata (100% of organisms) and across the SK1-SK3 paralogs in other vertebrates. More precisely, a phenylalanine is present in 94.5% (479/507) of organisms encoding SK1, 86.7% (472/543) of those encoding SK3, and 83.8% (477/569) of those encoding SK2. In addition, in SK1 paralogs, a phenylalanine is observed in combination with other residues or ambiguous states (i.e., multi-copy genes) within the same organism in 3.7% (19/507) of cases, whereas this proportion reaches 11.4% in SK3. Interestingly, in SK2 paralogs, tyrosine is the most frequent alternative residue found in 14.1% (80/569) of organisms, all belonging to the Actinopterygii lineage. In contrast, a tyrosine is observed in only two organisms encoding SK1 and in a single organism encoding SK3, all of which also belong to the Actinopterygii lineage.

Regarding SK4, which was included in this phylogenetic analysis despite its very different S3-S4 loop because it is part of the evolutionary history of the SK gene family, 95.6% (240/251) of organisms encoding this paralog display an ambiguous or missing state at this position, while a tyrosine is observed alone or in combination with an ambiguous state in 3.6%

(9/251) of cases. In one Latimeria organism (e.g., coelacanth), SK4 harbors a tyrosine in combination with an ambiguous state (i.e., multi-copy genes).

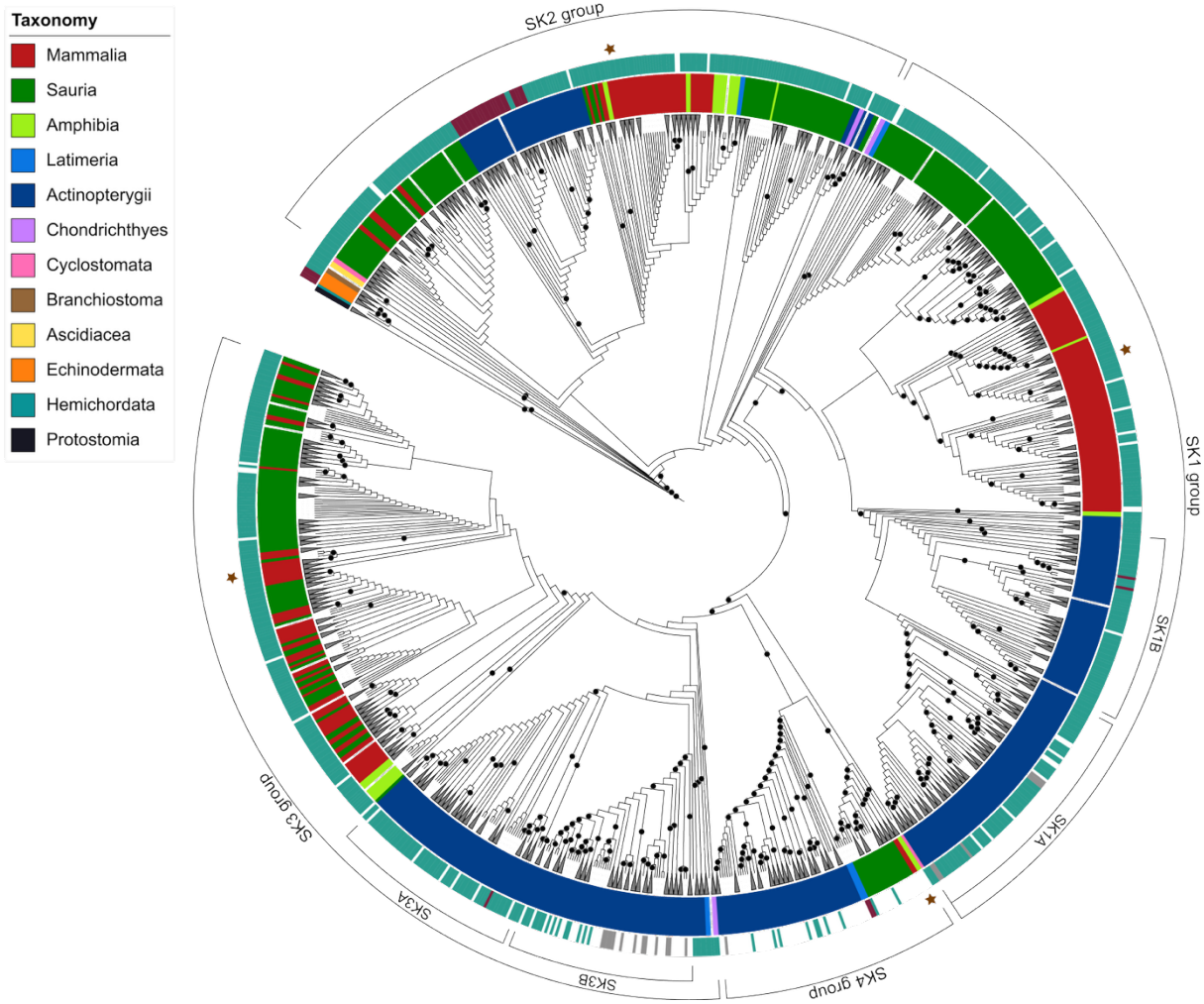

Figure 1. Circular phylogenetic tree of SK channels. The tree does not contain branch lengths, nodes are collapsed if the sequences have the same taxonomy (see legend) and the same mutation (F, Y or other), black circles indicate bootstraps ≥70. The first inner circle corresponds to the species taxonomy (see legend for details, white = undefined), the second circle highlights residue present at the tip of the S3-S4 loop (turquoise = F, burgundy = Y, other amino acids= gray and gap or ambiguous=white), and the last circle corresponds to the SK type. Positions of the human SK1, 2, 3, and 4 are marked with stars.

Determination of the affinity of apamin for the SK2 and SK3 mutants

Because this phylogeny of SK channels further highlight the importance of the phenylalanine residue at the tip of the S3–S4 β-hairpin loop, we chose to experimentally assess its role in SK2 and SK3 using alanine mutants, which would likely be disruptive, and tyrosine mutants, which represents the most common alternative to the phenylalanine observed in the phylogeny. We first evaluated the impact of both mutations on the affinity of apamin for SK2 and SK3 channels by doing a screening with 5 pM radiolabeled ^{125}I-apamin as described in the

methods. The results are shown in Table 1 where the specific binding is obtained by subtracting the measured non-specific binding from total binding (radioactive activity expressed in degradations per minute, dpm). As expected, mutation of the phenylalanine residue to alanine resulted in a loss of binding of ^{125}I-apamin to SK2 (specific binding = 31 ± 93 dpm for SK2 F243A vs 4106 ± 270 for SK2 WT ; n = 4) and SK3 channels (147 ± 155 dpm for SK3 F392A vs 4321 ± 304 dpm for SK3 WT ; n = 4). However, the results obtained for tyrosine mutants differ in SK2 and SK3. In SK2, the tyrosine mutation had no impact on the binding of radiolabeled apamin (specific binding = 5602 ± 224 dpm; n = 4), unlike SK3 where the same mutation greatly reduced the binding of the ligand to the channel (21 ± 105 dpm; n = 4). We repeated the experiment with the SK3 F392Y channel using a higher concentration of radiolabeled apamin (100pM) but the results still showed no binding of the ligand to the mutated channel (data not shown).

A saturation assay was performed on the SK2 F243Y channel to measure the dissociation constant (K_D) of apamin for this mutant and compare it to that of the WT SK2 channel (Fig. 2). The K_D of apamin were respectively 5,19 ± 1,96 pM and 4,31 ± 0,53 pM for WT and SK2 F243Y channels. Statistical analysis (Mann-Whitney test) did not detect any effect of the mutation at the given sample size (p = 0.7 ; n = 3 for each).

	Channels	SK2 WT	SK2 F243Y	SK2 F243A	SK3 WT	SK3 F392Y	SK3 F392A
Radioactivity (dpm)	Total Binding	4305 ± 239	5854 ± 245	298 ± 68	4660 ± 199	254 ± 69	385 ± 246
	Non Specific Binding	199 ± 35	252 ± 29	267 ± 45	340 ± 125	233 ± 40	238 ± 93
	Specific Binding	4106 ± 270	5602 ± 224	31 ± 93	4321 ± 304	21 ± 105	147 ± 155

Table 1. Screening of mutants compared to wild-type channels in *in-vitro* binding assay. Radioactivity is expressed in degradation per minute (dpm) and specific binding is obtained by subtracting the measured non-specific binding from total binding.

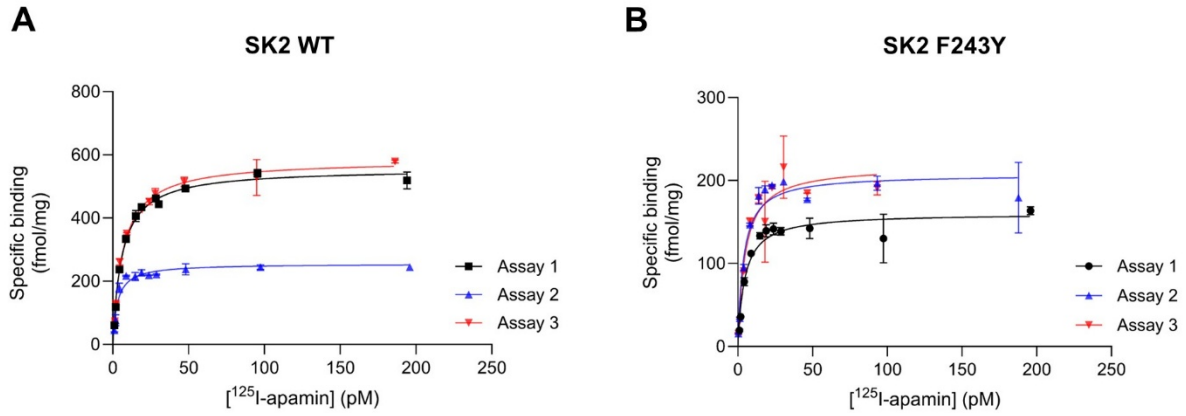

Figure 2. Saturation relationships for ^{125}I-apamin binding to expressed SK2 WT (A) or SK2 F243Y (B) subunits. The K_D of apamin for SK2 WT and SK2 F243Y are similar (p = 0.7 ; n = 3; Mann-Whitney test). Error bars correspond to the standard deviation (SD).

The sensitivity of the mutated channels to TEA remains unchanged compared to wild-type channels

TEA acts as a conventional potassium channel pore blocker by binding near the extracellular opening of the selectivity filter. It is commonly used to probe for structural changes in the outer pore region (20,49–52). In our initial patch clamp experiments, we applied TEA to verify that the channel mutations did not affect its sensitivity to the blocker. Any alteration in TEA responsiveness would indicate a significant conformational change or collapse of the channel pore.

As previously described (20,27,53), the expression of wild-type or mutated (alanine and tyrosine) SK2 and SK3 subunits produced inwardly rectifying currents in whole-cell recordings performed in symmetrical K^+ conditions and in the presence of 10 µM free Ca^{2+}. Currents were blocked by the application of increasing TEA concentrations (see Fig. S1 and S2 for raw current traces), and concentration-inhibition curves obtained after fitting the data with the Hill equation (Fig. 3). For SK2, the following IC_{50} values were respectively obtained for WT channels, the tyrosine mutant, and the alanine mutant: 5.91 ± 1.72 mM, 6.94 ± 1.46 mM, and 5.86 ± 0.48 mM (n=5 for each channel). For SK3, the values obtained were: 7.83 ± 2.09 mM (WT), 9.89 ± 2.37 mM (SK3 F392Y), and 8.42 ± 1.67 mM (SK3 F392A) (n=5). The fitted Hill coefficient (h) was around unity for each of the 6 channels tested (Table S1), in good agreement with findings from previous studies (20) and supporting the expected one-to-one binding interaction characteristic of a pore-blocking mechanism. Statistical analysis of IC_{50} values (Kruskal–Wallis test) did not detect any difference in sensitivity between wild-type and SK2 mutant channels (p = 0.74), or

between wild-type and SK3 mutant channels ($p = 0.83$), although the sample size may limit the detection of subtle effects.

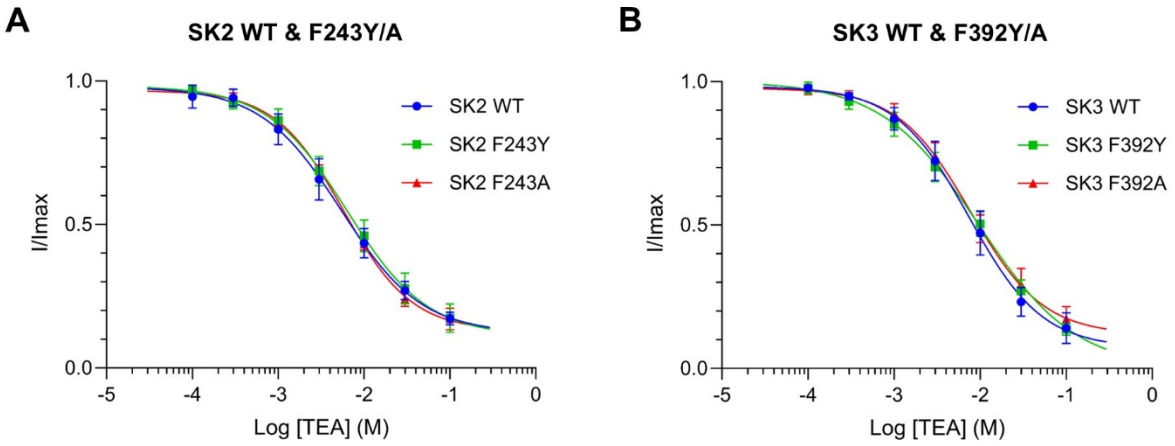

Figure 3. Patch clamp concentration-inhibition curves of TEA on SK2 (A) and SK3 (B). The sensitivity for wild-type channels and their SK2 F243A/Y and SK3 F392A/Y mutants are similar ($p > 0.05$; $n = 5$; Kruskal-Wallis test). Error bars correspond to the standard error of the mean (SEM).

Mutation of the conserved S3-S4 phenylalanine affects blockade by apamin

The importance of the unique S3-S4 phenylalanine for the efficacy of SK specific outer pore targeting blockers was further assessed, starting with the bee venom peptidic toxin apamin. Application of increasing concentrations of apamin led to the progressive inhibition of the currents measured in patch clamp experiments for HEK293 cells overexpressing SK2 WT and SK3 WT channels, as well as from their tyrosine mutants (Fig. 4A–D; see Fig. S3 and S4 for recordings on different cells). The IC_{50} values calculated from the concentration-inhibition curves are 220.5 ± 41.3 pM *(*$h = 1.68 \pm 0.11$, $n = 5$) for SK2 WT and 377.6 ± 94.7 pM ($h = 1.27 \pm 0.10$, $n = 5$) for SK3 WT (Fig. 4E-F, Table S1). Contrary to previous reports, our results do not reveal any significant difference between the IC_{50} values of these two channels within the limits of our sample size, although a trend is noted ($p = 0.22$, Mann-Whitney test), with SK3 exhibiting greater sensitivity than previously documented (20,26,27). For SK2 F243Y, we obtained an IC_{50} of 226 ± 37.7 pM *(*$h = 1.20 \pm 0.09$, $n = 5$), similar to that of the SK2 WT (Fig. 4E, $p > 0.99$). Surprisingly, and in contradiction with the absence of binding observed during the screening of mutants, we observed a current block for the SK3 F392Y channel. However, unlike in SK2, a significant increase of the IC_{50} value for SK3 F392Y (2.03 ± 0.25 nM; $h = 1.05 \pm 0.12$, $n = 5$) was observed compared to that for SK3 WT (Fig. 4F, $p = 0.008$).

Because SK2 F243A and SK3 F392A did not exhibit any binding to radiolabeled apamin in the binding assays, we applied a supramaximal concentration of apamin (1 µM) in the patch-

clamp experiments. As anticipated, no current blockage was observed in either case (Fig. 4G-H). The average inhibition of current at -80 mV was -2.1 ± 6.8% for SK2 F243A (n = 5) and 1.2 ± 3.6% for SK3 F392A (n = 4). The minor variations observed are likely due to a slight fluctuation in current intensity over the period of the experiment rather than to an effect of apamin. Taken together, these results confirm the importance of the phenylalanine residue of the S3-S4 loop in the binding and blocking mechanisms by apamin.

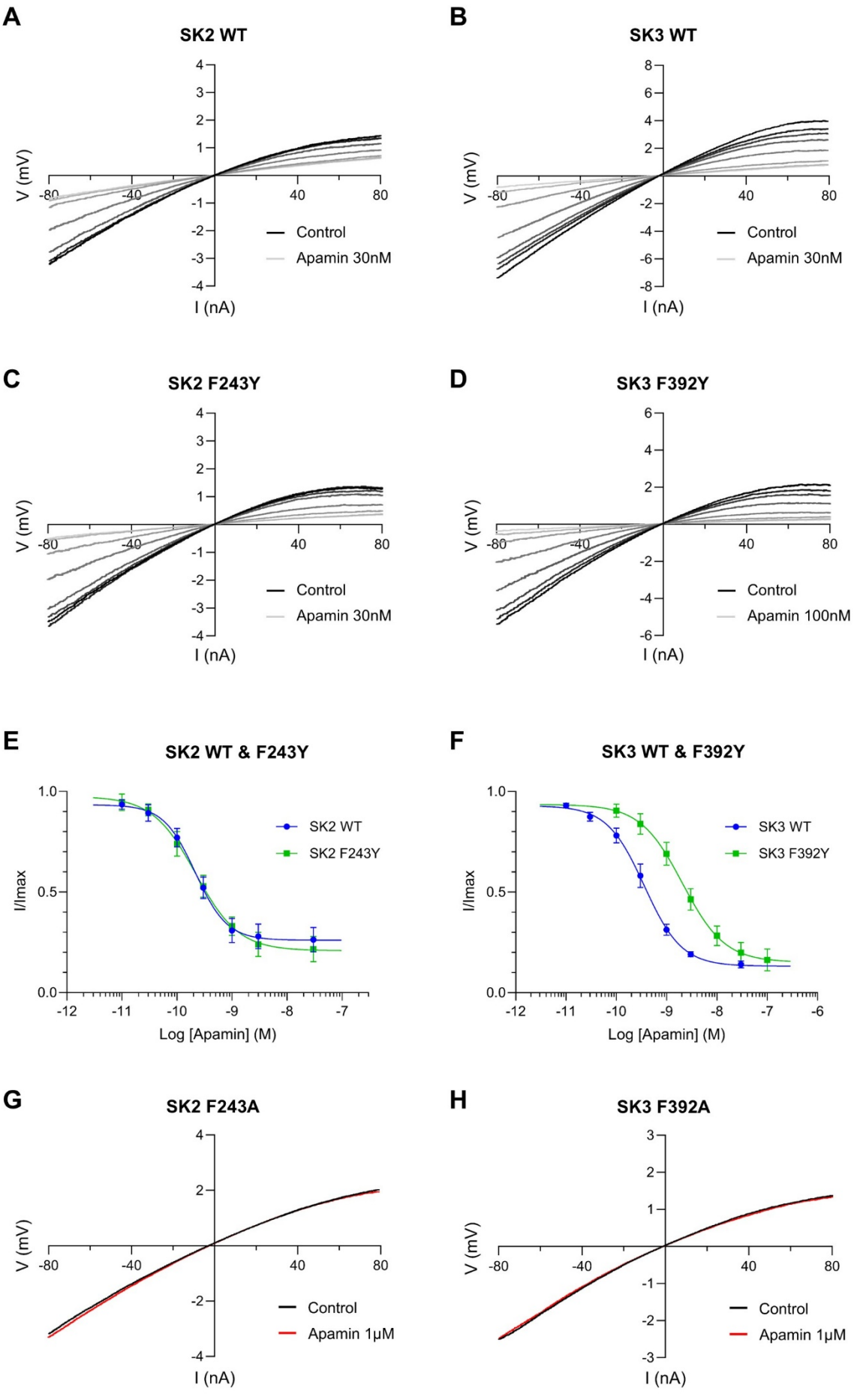
A
SK2 WT
V (mV)
I (nA)
Control
Apamin 30nM
B
SK3 WT
V (mV)
I (nA)
Control
Apamin 30nM
C
SK2 F243Y
V (mV)
I (nA)
Control
Apamin 30nM
D
SK3 F392Y
V (mV)
I (nA)
Control
Apamin 100nM
E
SK2 WT & F243Y
I/Imax
Log [Apamin] (M)
SK2 WT
SK2 F243Y
F
SK3 WT & F392Y
I/Imax
Log [Apamin] (M)
SK3 WT
SK3 F392Y
G
SK2 F243A
V (mV)
I (nA)
Control
Apamin 1μM
H
SK3 F392A
V (mV)
I (nA)
Control
Apamin 1μM

Figure 4. Effect of the S3-S4 phenylalanine mutations on blocking by apamin in whole-cell patch clamp experiments. (**A-D**) Representative I–V relationships measured from whole-cell recordings obtained from HEK293 cells expressing SK2 WT, SK3 WT, SK2 F243Y or SK3 F392Y channels, in the absence (control, black line) or in the presence of increasing concentrations of apamin, from the lowest concentration (dark grey line) to the highest concentration (light grey line). For SK2 WT, SK3 WT and SK3 F243Y, the apamin concentrations used were 10 pM, 30 pM, 100 pM, 300 pM, 1 nM, 3 nM and 30 nM. For SK3 F392Y, the apamin concentrations were 100 pM, 300 pM, 1 nM, 3 nM, 10 nM, 30 nM and 100 nM. (**E**) Concentration-inhibition curves of apamin for SK2 WT and SK2 F243Y, error bars correspond to the standard error of the mean (SEM). (**F**) Same for SK3 WT and SK3 F392Y. (**G-H**) I–V relationships measured from whole-cell recordings obtained from HEK293 cells expressing SK2 F243A (n = 5) or SK3 F392A (n = 4) channels, in the presence (red line) or absence (black line) of apamin 1μM.

Mutation of the conserved S3-S4 phenylalanine affects blocking by UCL1684

UCL1684 displaces apamin from its binding to the channel outer pore region (25,54). It is therefore possible that the mutations of the phenylalanine generated in this study also have an impact on the interaction between SK subtypes and the bisquaternary compound. As with apamin, the application of increasing concentrations of UCL1684 led to the inhibition of wild-type and tyrosine mutant channels (Fig. 5A–D; see Fig. S5 and S6 for recordings on different cells). The IC_{50} values determined for the SK2 WT and SK3 WT current inhibition by UCL1684 (Fig. 5E-F, Table S1) were respectively 365.9 ± 55.9 pM *(h* = 0.89 ± 0.06) and 411.2 ± 98.3 pM (*h* = 0.60 ± 0.04,). Statistical analysis ($p > 0.99$; n = 5) did not provide evidence for a difference between these values. Experiments on tyrosine mutants also revealed similar results with the following IC_{50} for SK2 F243Y and SK3 F392Y respectively: 457.5 ± 81.6 pM *(h* = 0.73 ± 0.06, *n* = 5) and 380.4 ± 51.6 pM (*h* = 0.60 ± 0.07, *n* = 5). The IC_{50} of UCL1684 were comparable for wild type and tyrosine mutant channels in both SK2 and SK3 ($p = 0.55$ for SK2 channels and $p > 0.99$ for SK3 channels). In contrast to what we observed for the SK3 tyrosine mutant in the apamin experiments, we did not observe a statistically significant difference in the block by UCL1684 of the tyrosine mutant and the wild-type channel.

For the SK2 F243A and SK3 F392A mutants, similarly to our experiments with apamin, we assessed their activity using a supramaximal concentration (1 μM) of UCL1684 (Fig. 5G-H). The findings indicated that these alanine mutants are insensitive to UCL1684, with average current inhibition of 5.2 ± 1.7% for the SK2 F243A channel (n = 5) and 1.1 ± 2.6% for SK3 F392A (n = 5). These results further confirm that the phenylalanine residue in the S3-S4 loop is crucial for the binding and blocking not only by apamin but also by UCL1684. Table S1 summarizes the IC_{50} values and Hill coefficients obtained for each channel tested with each of the compounds.

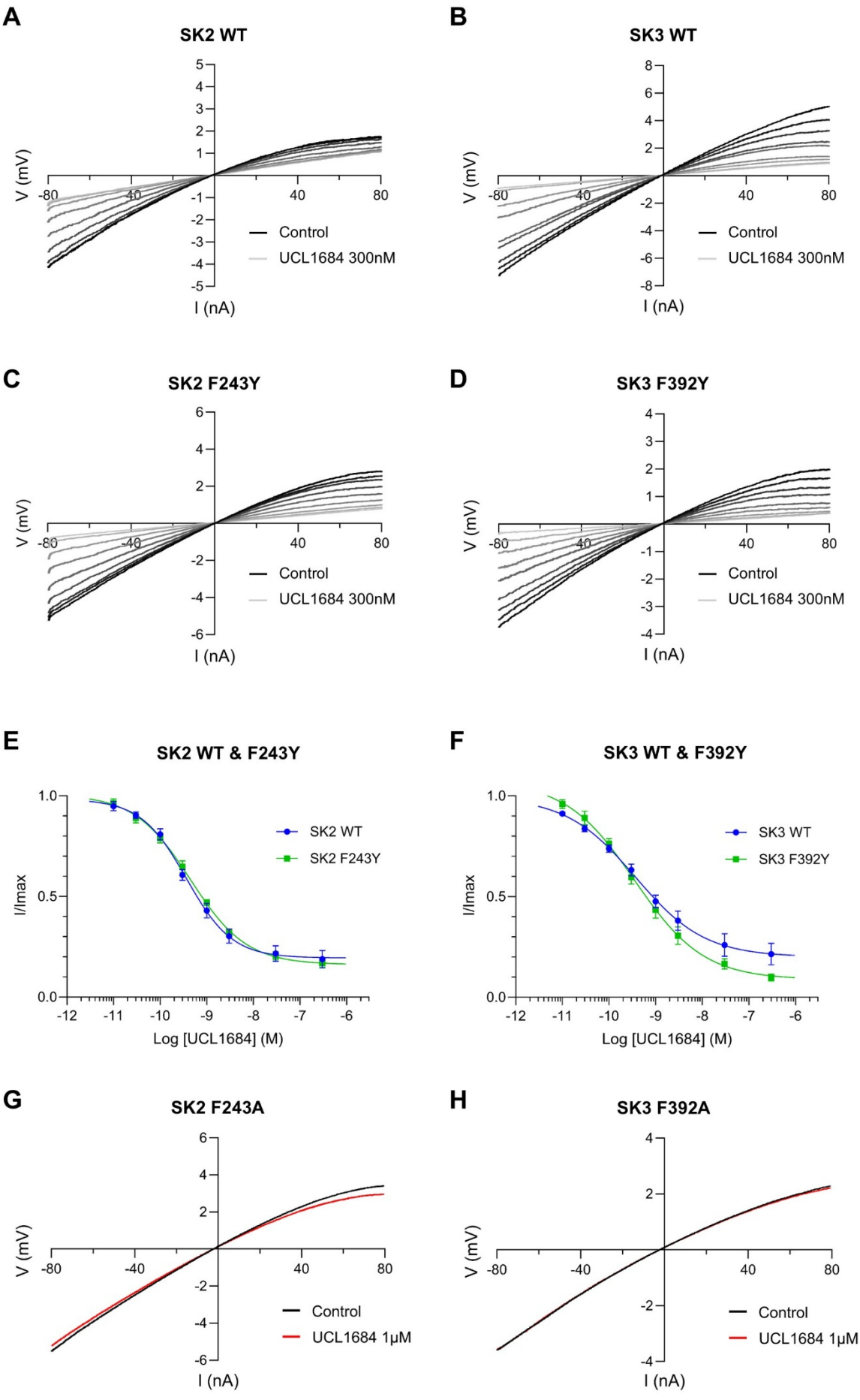
A
SK2 WT
V (mV)
I (nA)
Control
UCL1684 300nM
B
SK3 WT
V (mV)
I (nA)
Control
UCL1684 300nM
C
SK2 F243Y
V (mV)
I (nA)
Control
UCL1684 300nM
D
SK3 F392Y
V (mV)
I (nA)
Control
UCL1684 300nM
E
SK2 WT & F243Y
I/Imax
Log [UCL1684] (M)
SK2 WT
SK2 F243Y
F
SK3 WT & F392Y
I/Imax
Log [UCL1684] (M)
SK3 WT
SK3 F392Y
G
SK2 F243A
V (mV)
I (nA)
Control
UCL1684 1μM
H
SK3 F392A
V (mV)
I (nA)
Control
UCL1684 1μM

Figure 5. Effect of the S3-S4 phenylalanine mutations on blocking by UCL1684 in whole-cell patch clamp experiments. (**A-D**) Representative I–V relationships measured from whole-cell recordings obtained from HEK293 cells expressing SK2 WT, SK3 WT, SK2 F243Y or SK3 F392Y channels, in the absence (control, black line) or in the presence of increasing concentrations of UCL1684, from the lowest concentration (dark grey line) to the highest concentration (light grey line). The UCL1684 concentrations used were 10 pM, 30 pM, 100 pM, 300 pM, 1 nM, 3 nM, 30 nM and 300 nM. (**E-F**) Concentration-inhibition curves show similar sensitivity to UCL1684 for wild-type and tyrosine mutant in both SK2 and SK3 ($p > 0.05$; $n = 5$; Mann-Whitney test). Error bars correspond to the standard error of the mean (SEM). (**G-H**) I–V relationships measured from whole-cell recordings obtained from HEK293 cells expressing SK2 F243A ($n = 5$) or SK3 F392A channels ($n = 5$). Each I–V plot shows an averaged control trace (black) and an averaged trace obtained in the presence of UCL1684 1µM.

Modeling of the SK2 F243Y and SK3 F392Y mutants

To further investigate the impact of the phenylalanine to tyrosine mutation, structural models of tyrosine mutants in SK2 and SK3 were generated using AlphaFold3, with the SK2 wild-type structure (pdb_00008v2g) serving as unique template to preserve the low conductance conformation of the selectivity filter. The overall ranking score were respectively 0.88 and 0.89 for SK2 F243Y and SK3 F392Y models. The average pLDDT for residues present in the model are 82.3 and 82.7 respectively (Fig. S7). This setup allowed the prediction of the specific low conductance conformation of the selectivity filter observed in the SK2 structure (Fig. 6). The rms deviation calculated for all Cα between any SK molecule of the SK2 structure and the SK2 F243Y or SK3 F392Y models are respectively 1.6 Å and 1.7 Å.

In these models, the hydrophobic interactions of the S3-S4 phenylalanine previously shown to induce conformational changes in the SK2 selectivity filter is maintained by the substituting tyrosine and this residue forms an additional hydrogen bond with the carbonyl group of the second glycine of the selectivity filter GYG motif (G362 in SK2, G511 in SK3). These hydrogen bonds are 2.8 Å and 2.6 Å long in SK2 and SK3 respectively and are ideally oriented within the same monomer (Fig. 6C-D). This additional interaction potentially enhances the stability of the S3–S4 loop conformation.

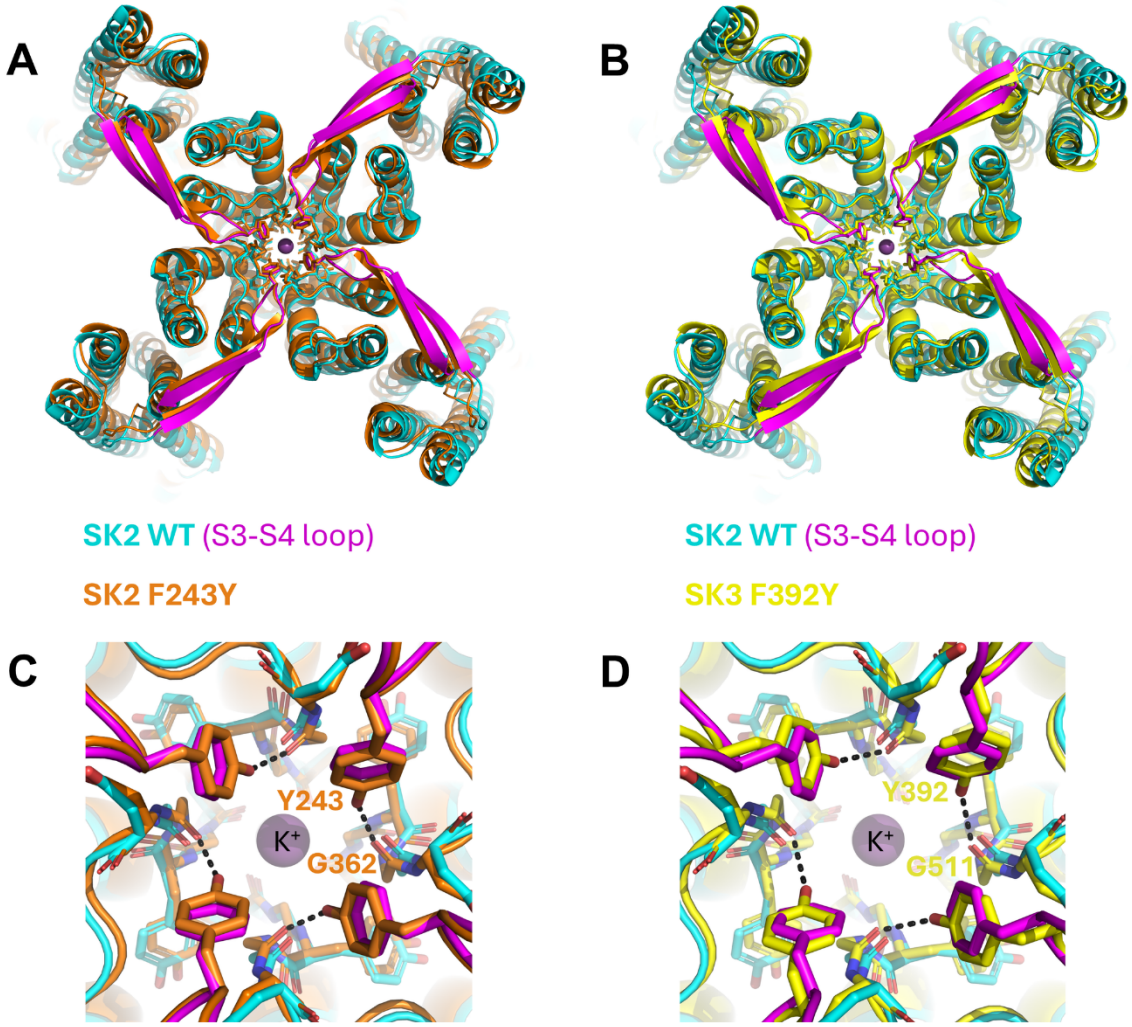

Figure 6. Models of the SK2 F243Y and SK3 F392Y mutants. (A-B) Extracellular view of the SK2 F243Y and SK3 F392Y models (respectively in orange and yellow) superimposed on SK2 WT structure – pdb_00008v2g (cyan). S3-S4 loop of SK2 WT is shown in magenta. (**C-D**) Zoom on the on the pore exit of the channels. The hydrogen bonds between Y243 and G362 in SK2, and Y392 and G511 in SK3 are shown as black dashed lines.

Determination of the potential binding mode of TEA by docking

To gain further insight into the interaction between TEA and SK channels, molecular docking was first performed on the wild-type SK2 channel structure (pdb_00008v2g) using the AutoDock Vina algorithm. The two top-scoring binding poses (Fig. 7A) position TEA at the extracellular pore entrance: either adjacent to the conserved phenylalanine residues within the S3-S4 loops (pose 1), or within the negatively charged region formed by the carbonyl groups of the selectivity filter (pose 2). While pose 2 exhibits a more favorable binding energy (-3.95 kcal/mol; K_D: 1.27 mM), Pose 1 (-3.41 kcal/mol; K_D: 3.15 mM) seems to be more plausible. The steric bulk of TEA seems to prevent it from penetrating between the phenylalanine side chains to access the selectivity filter directly. Such access would require conformational

flexibility in the S3-S4 loop, which appears unlikely given the low B-factors observed in the SK2 experimental structure and the molecular dynamics simulation previously performed (31). However, previous whole-cell patch clamp experiments recording the current induced at -80 mV upon apamin addition after incubation with 1.8mM TEA have suggested that the apamin and TEA sites on SK3 are distinct (20). This absence of competition between these blockers would therefore be in better agreement with pose 2.

To support our experimental observations and assess whether TEA remains localized in the pore when the S3-S4 loop becomes unstructured—a condition we hypothesize arises from phenylalanine-to-alanine substitution—we conducted additional docking simulations using the recently solved structure of the SK2 F243S mutant (pdb_00009eio), which should be structurally comparable to the alanine mutant. The most favorable binding pose (Fig. 7B) was located at the pore exit, occupying an intermediate position between Poses 1 and 2 seen in the wild-type channel. The associated binding energy and K_D were -2.58 kcal/mol and 12.80 mM, respectively. These values are of the same order of magnitude as those obtained for the wild type channel but seem to indicate a slight decrease in the affinity of TEA for the channel.

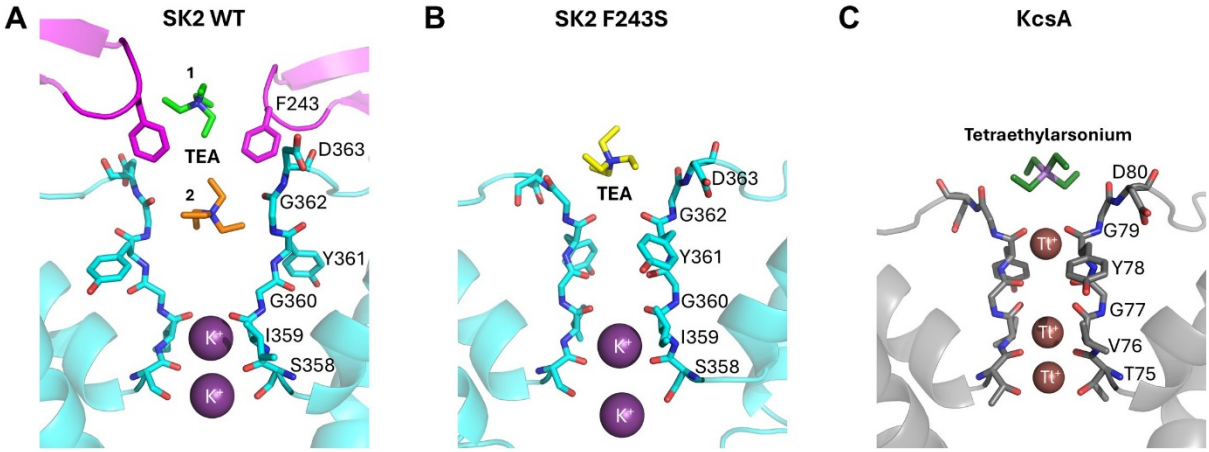

Figure 7. Docking of TEA on SK2 channel. (**A**) Side view of the two poses (pose 1 in green and pose 2 in orange) obtained for the docking of TEA on SK2 WT channel. Residues composing the selectivity filter (cyan) and the phenylalanine of the S3-S4 loops (magenta) are shown as sticks. (**B**) Side view of the pose obtained for the docking of TEA on SK2 F243S channel. Residue numbering was adjusted to match the human form of the protein. (**C**) Side view of the KcsA structure (pdb_00002boc) complexed with tetraethylarsonium in the presence of thallium ions. In each panel, only two monomers of the channels are displayed for clarity.

Molecular dynamic simulations of K^+ permeation through mutated SK channels

All-atom MD simulations were performed to assess K^+ permeation through the pores of SK2 and SK3, as well as of their variant with the S3-S4 loop phenylalanine substituted by an alanine or a tyrosine with a setup similar to that of Nam *et al (31)*. We followed K^+ permeation

events through the selectivity filter of SK channels embedded in lipid bilayers in the presence of a symmetric 300 mM KCl aqueous solution and a transmembrane voltage potential of 300 mV during 1-μs-long simulations. The inner gate was kept open throughout the simulation with restraints on the conserved gate valine and the two adjacent residues. For each channel, three trajectories were generated starting from the same initial state but with a different set of random velocities for the atoms. For SK2, the experimental structure (pdb_00008v2g) was used as starting point, while the AlphaFold model was used in every other case (based on the 8v2g structure for SK2 F243Y, SK3 WT and SK3 F392Y, and based on the 9eio structure for SK2 F243A and SK3 F392A). Measurement of the distance between the Cα of the S3-S4 loop phenylalanine (or its substituted residue) from opposite molecule and between the Cα of the tyrosine residue of the selectivity filter from opposite molecules, as well as the evolution of the RMSD calculated for the backbone atoms of all amino acid in the system show a good overall stability throughout the 1 μs duration of the simulations (Fig. S8-S13).

For SK2 WT and SK3 WT, the average number of permeation events calculated for the three replicates are similar, 13 ± 7 and 16 ± 4 respectively (Fig. 1, S8 and S11). For the tyrosine mutants, the values are also in the same range, with 16 ± 6 and 10 ± 3 for SK2 F243Y and SK3 F392Y respectively (Fig. 1, S9 and S12, supplemental movie 1-2). However, for the alanine mutants the average number of permeation events greatly increases to 46 ± 4 and 58 ± 19 for SK2 F243A and SK3 F392A respectively (Fig. 1, S10 and S13, supplemental movie 3-4), as observed for the serine mutant (31).

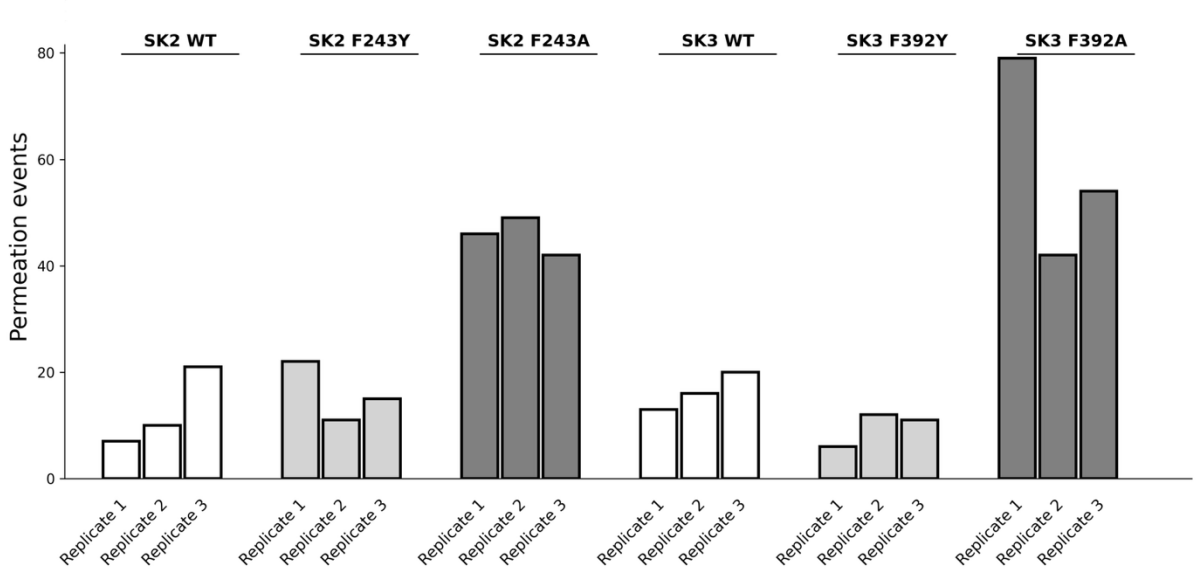

Figure 1. K^+ permeation events detected during MD simulations. Count of K^+ ions going through the selectivity filter of SK2 WT, SK2 F243Y, SK2 F243A, SK3 WT, SK3 F392Y and SK3 F392A during 1μs MD simulations. Each simulation was replicated three times.

Discussion

Effect of the S3-S4 phenylalanine mutations on the SK2 and SK3 structures

In the absence of experimental data on the structure of the mutated SK channels used in the present study, we relied on *in silico* predictions generated with the AlphaFold3 software (40). However, the only conditions in which we were able to generate models with the specific conformation of the selectivity filter observed in the WT SK2 structure, is by running AlphaFold3 with the latter structure as unique template. This strategy was therefore used to generate the models of SK3 WT and the SK2 and SK3 tyrosine mutants. Consequently, these models are not independent proof of the structure of these mutants, but an illustration of the potential effect induced by the replacement of the S3-S4 phenylalanine by a tyrosine. The probability that these models are correct is however high because the hydrophobic interactions mediated by the phenylalanine which induce the conformation of the selectivity filter is fully conserved with the tyrosine. Furthermore, the hydroxyl group of the latter does not generate steric hindrance or electrostatic repulsion but provides an ideal H-bond with the second glycine of the selectivity filter (Fig. 6), which further stabilizes the observed conformation of the S3-S4 loop responsible for the small current of SK channels (31).

For the alanine mutants, we expect the same destabilization of the S3-S4 loop as the one observed for the SK2 F243S mutant (31), and therefore the same return to the canonical conformation of the selectivity filter. Because the S3-S4 loop is not defined in the SK2 F243S structure, it very likely also represents the structure of the SK2 F243A mutant.

Low IC_{50} values for the blockage of SK3 by apamin and UCL1684

While the IC_{50} values obtained for SK2 WT with apamin and UCL1684 are consistent with those reported in the literature, the values calculated for SK3 WT with both compounds are slightly lower than previously published data. For apamin, reported IC_{50} values for SK3 vary considerably, ranging from 630 pM to 19 nM (23,55,56), placing our measured value (377.6 ± 94.7 pM) not far outside that range. In contrast, reported IC_{50} values for UCL1684 generally fall within the low nanomolar range (2.7–9.5 nM) (26,57), whereas our measured value is approximately tenfold lower (411.2 ± 98.3 pM)

At present, we do not have a definitive explanation for this discrepancy. The results were highly reproducible over several weeks, and experiments on SK3 were performed in

parallel with those on SK2, limiting the likelihood of systematic experimental bias. In addition, the IC_{50} values obtained with TEA are in good agreement with previously published data (20,23,27), supporting the overall reliability of our measurements. Finally, extra verifications were carried on to ensure that the protocol didn't include any error and that the correct plasmid was used for transfection.

TEA blocking and S3-S4 phenylalanine mutations

Electrophysiological experiments with TEA showed that substitution of the conserved S3–S4 loop phenylalanine with an alanine or a tyrosine in SK2 and SK3 channels did not seem to alter their sensitivity to the blocker (Fig. 3 and Table S1). All channel variants exhibited concentration–response curves with IC_{50} values in the millimolar range, and no statistically significant differences were observed between a wild-type channel and its mutants. To further investigate TEA binding, molecular docking was performed using the SK2 WT structure (pdb_00008v2g)(31). Two binding sites were identified at the extracellular pore entrance: one adjacent to the S3–S4 phenylalanine side chains and another within the widened outer selectivity filter. Although the latter had a more favorable binding energy (–3.95 kcal/mol), steric hindrance likely limits TEA access to this site, making the first pose more likely. Docking simulations using the structure of a SK2 F243S channel (pdb_00009eio) as a surrogate for alanine mutants, revealed a binding location between the four G362 and D363 residues at the exit of the selectivity filter, similar to the one observed in the structure of the KcsA K^+ channel in complex with tetraethylarsonium, a TEA analogue (Fig. 7B-C) (51). The calculated K_D from docking experiments are of the same order of magnitude (mM range) as the experimentally determined IC_{50} values, reinforcing the relevance of the predicted docking poses. The fine fluctuations between the K_D related to the SK2 WT and the mutants do however not match the experimentally determined IC_{50} values.

UCL1684 blocking and S3-S4 phenylalanine mutations

Two cryo-EM structures of SK2 in complex with UCL1684 have recently showed the importance of the S3-S4 phenylalanine for the binding of this compound (31,33). This result was confirmed with both SK2 F243A and SK3 F392A mutants which were entirely insensitive to UCL1684 in whole cell patch clamp experiments. For the tyrosine mutants, IC_{50} values remained in the hundreds picomolar range, and the analysis did not provide evidence for an effect in either SK2 F243Y or SK3 F392Y, suggesting that this substitution does not markedly

disrupt interaction with the compound. This is a strong indication that the specific conformation of the S3-S4 loop is not affected in the SK2 F243Y and SK3 F392Y mutants.

Note that UCL1684 inhibition curves yielded an apparent Hill coefficient lower than 1, indicating a shallower slope than expected for a simple one-site interaction. This is unlikely to result from experimental artefacts, as TEA and apamin displayed Hill coefficients close to unity under identical conditions. The origin of this reduced slope remains unclear, although Hill slope lower than 1 have occasionally been reported for UCL1684 on SK channels (58).

Apamin blocking and S3-S4 phenylalanine mutations

As highlighted by the two recent cryo-EM structures, the apamin interaction with SK2 is highly dependent of on two π-cation interactions between the apamin R13 and R14 and the S3-S4 phenylalanine residue of two opposite SK2 molecules of the channel. This interaction induces a transition between the low conductance conformation of the selectivity filter observed in the 8v2g SK2 structure and the canonical conformation of the selectivity filter present in the SK2-apamin complex (32,33). Radioligand binding assays using ^{125}I-apamin showed that alanine substitution at this position abolishes apamin binding in both SK2 and SK3 channels, functionally leading to an absence of current blockage as shown in whole cell patch clamp experiments for apamin concentration up to 1 µM.

Substitution of the S3-S4 phenylalanine with a tyrosine however produces more nuanced effects. SK2 F243Y binds apamin with an affinity comparable to the SK2 WT and in whole cell patch clamp experiments, the current flowing through these two channels is blocked by apamin with similar IC_{50} values in the low hundreds picomolar, indicating that, in SK2, the tyrosine substitution does not impact apamin binding and its functional blockade.

For SK3, the SK3 F392Y mutant failed to bind apamin, even with a 20-fold increased ligand concentration and despite several attempts with different batches of membrane preparation. Additionally, in the functional assay, SK3 F392Y showed an approximately 5-fold increase in IC_{50} compared to SK3 WT. These results point to a significantly lower affinity of apamin for SK3 F392Y. The 3D models obtained for SK2 F243Y and SK3 F392Y show that in these mutants the stability of the S3-S4 loop could be increased because of the additional H-bond formed by the tyrosine hydroxyl group and the carbonyl of the second glycine of the selectivity filter GYG motif (Fig. 6C and D). A higher stabilizing impact of this H-bond in SK3 could slightly prevent the conformational change induced upon binding of apamin, potentially leading to the lower affinity observed.

Evolutionary history of the SK gene family in vertebrates

The overall topology of the SK phylogenetic tree is consistent with current models of vertebrate gene evolution. In fact, it was proposed that vertebrate evolution has been driven by a whole-genome tetraploidization event that occurred more than 450 million years ago in an early vertebrate lineage (59,60). However, the precise timing of the two rounds of vertebrate whole-genome duplication remains debated. Two main hypotheses have been proposed: (i) both duplication events occurred early in vertebrate evolution, prior to the last common ancestor of vertebrates, or (ii) the first duplication occurred prior to the last common ancestor of vertebrates, whereas the second occurred separately after the split between agnathans (jawless fishes) and gnathostomes (jawed vertebrates) lineages (61).

Our phylogenetic analysis supports the second scenario, where all four SK paralogs are represented exclusively by sequences from jawed vertebrates, including Chondrichthyes, Actinopterygii, Latimeria, Amphibia, Sauria, and Mammalia. In contrast, sequences identified in jawless fishes (i.e., Cyclostomata) are restricted to two paralogous lineages: one positioned at the base of the SK3-SK4 subtree, and the second grouping close to the basal deuterostome sequences (i.e., Hemichordata, Echinodermata, Branchiostoma, and Ascidiacea), at the base of the larger subtree encompassing all four SK paralogs (Fig. 1). Nevertheless, the alternative scenario cannot be excluded. Indeed, some jawless fish species have undergone extensive gene loss during their evolutionary history (62) and their relatively low extant species diversity (63) may also contribute to the observed topology.

Regarding Chondrichthyes (cartilaginous fishes), our analyses do not recover the SK4 paralog. This absence may reflect incomplete or fragmented genome assembly, along with limited representation in public genomic databases (64). However, lineage-specific loss of this paralog in early chondrichthyans cannot be ruled out.

In addition to the two whole-genome duplications that occur early in vertebrate evolution, a third whole-genome duplication occurs later in teleost fishes, a major subdivision of Actinopterygii, around 286-267 million years ago (61,65,66). Consequently, additional paralogs are observed within SK1 (named SK1A and SK1B) and SK3 (SK3A and SK3B) subtrees (Fig. 1), resulting in up to six SK copies in some teleost genomes. Because teleost fishes subsequently lost an estimated 70-80% of duplicated genes following this whole-genome duplication (65), we assume that additional SK2 and SK4 copies were likely lost during this period.

Analysis of the residue located at the tip of the S3–S4 loop showed that phenylalanine is the predominant amino acid across deuterostome sequences. However, a few natural

substitutions are occasionally observed, with tyrosine being the most frequent alternative residue. The tyrosine form is mainly found in the SK2 paralog within Actinopterygii. Outside vertebrates, a tyrosine is also observed in basal deuterostomes (Hemichordata and Echinodermata). Because only a single Hemichordata sequence is available, and both phenylalanine and tyrosine residues are present in Echinodermata, it remains unclear whether the phenylalanine or tyrosine represents the ancestral state of the SK channel. In vertebrates, the tyrosine form is rarely observed in SK1, SK3 and SK4 paralogs. Actinopterygian species typically harbor either the phenylalanine or the tyrosine form of SK2, but rarely both, supporting a phenylalanine to tyrosine substitution at the base of the actinopterygian SK2 lineage followed by lineage-specific reversions.

Interestingly, residue analysis reveals that the S3-S4 loop region is highly divergent in all SK4 paralogs and in the additional SK3 (SK3B) paralog identified in teleost fishes, suggesting a functional shift in these channels. While such divergence is consistent with the known functional properties and structure of SK4(4), the functional divergence of the actinopterygian SK3B paralog remains unknow.

Physiological effect of a tyrosine the tip of the S3-S4 loop

The S3-S4 loop and in particular its tip phenylalanine have been linked to a SK specific low conductance conformation of the selectivity filter(31). This result was validated by the study of a SK2 channel with the phenylalanine substituted into a serine which displayed a higher single channel current, a higher number of ion permeation events in MD simulations and an experimental structure with a canonical conformation of the selectivity filter. These results are in line with our MD simulations on SK2 F243A and SK3 F392A, which show a more than 3.5-fold increase in permeation events during 1 μs simulations compared to WT channels (Fig. 1). This suggest a similar impact of the alanine and serine mutations even if our simulations cannot be considered as independent validations because they are using an initial model that uses the SK2 F243S structure as template.

Phylogenic analysis of potassium channels containing the SK specific S3-S4 loop identified naturally occurring substitutions of the S3-S4 phenylalanine into a tyrosine. Because it very rarely occurs in the SK1 and SK3 groups of the tree, and it forms a monophyletic group in the Actinopterygii class of the SK2 group where most substitutions are observed, we wonder if this substitution is linked to specific properties of these SK channels. The more polar property of the tyrosine compared to the phenylalanine could indeed have a positive effect on the flow of K^+ ions through the channel. Comparison of the permeation events detected during the MD

simulations of the SK2 WT, SK2 F243Y, SK3 WT and SK3 F392Y did however not lead to the identification of a significant difference neither between a channel and its mutant nor between channel subtypes, likely indicating an absence of effect of the tyrosine mutation on the K^+ current.

Additionally, because of the additional H-bond between the tyrosine side chain and the selectivity filter (Fig. 6C and D), this mutation could impact the stability of the S3-S4 loop and consequently of the overall low conductance conformation of the channels. The advantage of having more stable SK channel could be crucial to maintain the SK functionality in a wider range of conditions or if the susceptibility to peptidic toxins like apamin is indeed reduced like we measured in the case of SK3 (Table 1 and Fig. 4F), the tyrosine mutation could have been selected as a mechanism of resistance in an Actinopterygii ancestor facing the challenge of toxin producing rival species.

Conclusions

This study focused on the functional and structural relevance of the S3–S4 β-hairpin loop of SK channels and the conserved phenylalanine present at its tip. Using site-directed mutagenesis, this phenylalanine was substituted with either alanine or tyrosine in both SK2 and SK3 subtypes. *In vitro* binding assays, in combination with electrophysiological recordings, demonstrated the essential role of this residue in mediating high-affinity interactions with the channel blockers UCL1684 and apamin. The tyrosine mutation does not affect current blockage by UCL1684. However, apamin blocking efficiency is reduced in the SK3 F392Y mutant, potentially highlighting a stabilization effect of the S3-S4 loop more pronounced in SK3 that could interfere with the apamin induced conformational change observed in the SK2:apamin structure.

The phylogeny of SK channels (SK1-4) presented is consistent with a model of vertebrate gene evolution driven by a whole-genome tetraploidization, with the first duplication occurring prior to the last common ancestor of vertebrates, and the second occurring separately after the split between agnathans (jawless fishes) and gnathostomes (jawed vertebrates) lineages. SK4 channels form a divergent group of paralogs presenting an early loss of the SK characteristic S3-S4 loop. The characteristic phenylalanine at the tip of this loop is the predominant amino acid across deuterostome sequences, with tyrosine being the most frequent alternative residue. The latter form is mainly found as the SK2 paralog within Actinopterygii. A tyrosine and phenylalanine are observed in basal deuterostomes; the ancestral state of this

position remains therefore undetermined. The tyrosine substitution does not significantly affect the current observed in MD simulations. The selection of the tyrosine mutation in Actinopterygii SK2 could have resulted from a lower susceptibility to peptidic toxins produced by rival species, as observed between human SK3 and apamin.

Data and code availability

All data needed to evaluate the conclusions in this paper are present in the main text, the supporting material or in the Figshare online open access repository (https://doi.org/10.6084/m9.figshare.31231342). Additional information related to this paper may be requested from the authors.

Author contributions

AM, VL, FK, JFL, VS and AB designed the research. AM, VL TN, AG, JFL and RV performed the research. AM, VL, AG, FK, JFL, VS and AB analyzed data. AM, VL AG, FK, JFL and VS wrote the manuscript. AM, VL and AG prepared the figures.

Declaration of interests

The authors declare no competing interests.

Acknowledgments

This work was supported by F.R.S.-FNRS grants "Crédit de recherche" (grant CDR/353230060 & 40028950) to J-F.L., a F.R.S.-FNRS grant "Crédit de recherche" (grant CDR/ J.0186.24) to V.S., a F.R.S.-FNRS grant "Projet de recherche" (grant PDR/T.0121.22) to F.K. and an "Action de Recherche Concertée" from Fédération Wallonie-Bruxelles (grant ARC 21/25-08). F.K. and J-F.L. are respectively Research Associate and Research Director of the F.R.S.-FNRS (Brussels, Belgium). Computational resources have been provided by the Consortium des Équipements de Calcul Intensif (CÉCI), funded by the Fonds de la Recherche Scientifique de Belgique (F.R.S.-FNRS) under Grant No. 2.5020.11 and by the Walloon Region. This research also benefited from computational resources made available on Lucia, the Tier-1 supercomputer of the Walloon Region, infrastructure funded by the Walloon Region under the grant agreement n°1910247.

Supporting material

Supplemental figures and tables

Supplemental movie 1. **Permeation event observed during the MS simulation of SK2 F243Y**. The video shows the 15 K^+ (red spheres) permeation events recorded during the 1 μs MD simulation. SK2 F243Y channel are represented in light green, yellow, light cyan and pink cartoon, and the Y243 side chain as sticks. Calmodulin molecules are shown as light blue cartoon, Ca^{2+} ions as green spheres and the membrane lipids head groups as grey sticks.

Supplemental movie 2. **Permeation event observed during the MS simulation of SK3 F392Y**. The video shows the 11 K^+ (red spheres) permeation events recorded during the 1 μs MD simulation. SK3 F392Y channel are represented in light green, yellow, light cyan and pink cartoon, and the Y392 side chain as sticks. Calmodulin molecules are shown as light blue cartoon, Ca^{2+} ions as green spheres and the membrane lipids head groups as grey sticks.

Supplemental movie 3. **Permeation event observed during the MS simulation of SK2 F243A**. The video shows the 46 K^+ (red spheres) permeation events recorded during the 1 μs MD simulation. SK2 F243A channel are represented in light green, yellow, light cyan and pink cartoon. Calmodulin molecules are shown as light blue cartoon, Ca^{2+} ions as green spheres and the membrane lipids head groups as grey sticks.

Supplemental movie 4. **Permeation event observed during the MS simulation of SK3 F392A**. The video shows the 54 K^+ (red spheres) permeation events recorded during the 1 μs MD simulation. SK3 F392A channel are represented in light green, yellow, light cyan and pink cartoon. Calmodulin molecules are shown as light blue cartoon, Ca^{2+} ions as green spheres and the membrane lipids head groups as grey sticks.

Declaration of generative AI and AI-assisted technologies in the manuscript preparation process

During the preparation of this work the authors used ChatGPT in order to improve the text of the manuscript. After using this tool/service, the authors reviewed and edited the content as needed and take full responsibility for the content of the published article.

References

1. Blatz AL, Magleby KL. Single apamin-blocked Ca-activated K+ channels of small conductance in cultured rat skeletal muscle. Nature. 1986 Oct 23;323(6090):718–20. doi:10.1038/323718a0 PubMed PMID: 2430185.

2. Park YB. Ion selectivity and gating of small conductance Ca(2+)-activated K+ channels in cultured rat adrenal chromaffin cells. J Physiol. 1994 Dec 15;481 (Pt 3)(Pt 3):555–70. doi:10.1113/jphysiol.1994.sp020463 PubMed PMID: 7707225; PubMed Central PMCID: PMC1155900.

3. Schumacher MA, Rivard AF, Bächinger HP, Adelman JP. Structure of the gating domain of a Ca2+-activated K+ channel complexed with Ca2+/calmodulin. Nature. 2001 Apr 26;410(6832):1120–4. doi:10.1038/35074145 PubMed PMID: 11323678.

4. Lee CH, MacKinnon R. Activation mechanism of a human SK-calmodulin channel complex elucidated by cryo-EM structures. Science. 2018 May 4;360(6388):508–13. doi:10.1126/science.aas9466 PubMed PMID: 29724949; PubMed Central PMCID: PMC6241251.

5. Köhler M, Hirschberg B, Bond CT, Kinzie JM, Marrion NV, Maylie J, et al. Small-conductance, calcium-activated potassium channels from mammalian brain. Science. 1996 Sep 20;273(5282):1709–14. doi:10.1126/science.273.5282.1709 PubMed PMID: 8781233.

6. Faber ESL, Sah P. Functions of SK channels in central neurons. Clin Exp Pharmacol Physiol. 2007 Oct;34(10):1077–83. doi:10.1111/j.1440-1681.2007.04725.x PubMed PMID: 17714097.

7. Sailer CA, Kaufmann WA, Marksteiner J, Knaus HG. Comparative immunohistochemical distribution of three small-conductance Ca2+-activated potassium channel subunits, SK1, SK2, and SK3 in mouse brain. Mol Cell Neurosci. 2004 Jul;26(3):458–69. doi:10.1016/j.mcn.2004.03.002 PubMed PMID: 15234350.

8. Tamarina NA, Wang Y, Mariotto L, Kuznetsov A, Bond C, Adelman J, et al. Small-conductance calcium-activated K+ channels are expressed in pancreatic islets and regulate glucose responses. Diabetes. 2003 Aug;52(8):2000–6. doi:10.2337/diabetes.52.8.2000 PubMed PMID: 12882916.

9. Skibsbye L, Poulet C, Diness JG, Bentzen BH, Yuan L, Kappert U, et al. Small-conductance calcium-activated potassium (SK) channels contribute to action potential repolarization in human atria. Cardiovasc Res. 2014 Jul 1;103(1):156–67. doi:10.1093/cvr/cvu121 PubMed PMID: 24817686.

10. Taylor MS, Bonev AD, Gross TP, Eckman DM, Brayden JE, Bond CT, et al. Altered expression of small-conductance Ca2+-activated K+ (SK3) channels modulates arterial tone and blood pressure. Circ Res. 2003 Jul 25;93(2):124–31. doi:10.1161/01.RES.0000081980.63146.69 PubMed PMID: 12805243.

11. Stocker M, Pedarzani P. Differential distribution of three Ca(2+)-activated K(+) channel subunits, SK1, SK2, and SK3, in the adult rat central nervous system. Mol Cell Neurosci. 2000 May;15(5):476–93. doi:10.1006/mcne.2000.0842 PubMed PMID: 10833304.

12. Rouchet N, Waroux O, Lamy C, Massotte L, Scuvée-Moreau J, Liégeois JF, et al. SK channel blockade promotes burst firing in dorsal raphe serotonergic neurons. Eur J Neurosci. 2008 Sep;28(6):1108–15. doi:10.1111/j.1460-9568.2008.06430.x PubMed PMID: 18783364.

13. Waroux O, Massotte L, Alleva L, Graulich A, Thomas E, Liégeois JF, et al. SK channels control the firing pattern of midbrain dopaminergic neurons in vivo. Eur J Neurosci. 2005 Dec;22(12):3111–21. doi:10.1111/j.1460-9568.2005.04484.x PubMed PMID: 16367777.

14. Adelman JP, Maylie J, Sah P. Small-Conductance Ca^{2+} -Activated K^{+} Channels: Form and Function. Annu Rev Physiol. 2012 Mar 17;74(1):245–69. doi:10.1146/annurev-physiol-020911-153336

15. Kshatri AS, Gonzalez-Hernandez A, Giraldez T. Physiological Roles and Therapeutic Potential of Ca2+ Activated Potassium Channels in the Nervous System. Front Mol Neurosci. 2018;11:258. doi:10.3389/fnmol.2018.00258 PubMed PMID: 30104956; PubMed Central PMCID: PMC6077210.

16. Grube S, Gerchen MF, Adamcio B, Pardo LA, Martin S, Malzahn D, et al. A CAG repeat polymorphism of KCNN3 predicts SK3 channel function and cognitive performance in schizophrenia. EMBO Mol Med. 2011 Jun;3(6):309–19. doi:10.1002/emmm.201100135 PubMed PMID: 21433290; PubMed Central PMCID: PMC3377084.

17. Sargin D, Oliver DK, Lambe EK. Chronic social isolation reduces 5-HT neuronal activity via upregulated SK3 calcium-activated potassium channels. Elife. 2016 Nov 22;5:e21416. doi:10.7554/eLife.21416 PubMed PMID: 27874831; PubMed Central PMCID: PMC5119885.

18. Diness JG, Sørensen US, Nissen JD, Al-Shahib B, Jespersen T, Grunnet M, et al. Inhibition of small-conductance Ca2+-activated K+ channels terminates and protects against atrial fibrillation. Circ Arrhythm Electrophysiol. 2010 Aug;3(4):380–90. doi:10.1161/CIRCEP.110.957407 PubMed PMID: 20562443.

19. Saljic A, Soattin L, Trachsel DS, Boddum K, Jespersen T. In vivo knockdown of SK3 channels using antisense oligonucleotides protects against atrial fibrillation in rats. J Mol Cell Cardiol. 2020 Oct;147:18–26. doi:10.1016/j.yjmcc.2020.07.011 PubMed PMID: 32768409.

20. Lamy C, Goodchild SJ, Weatherall KL, Jane DE, Liégeois JF, Seutin V, et al. Allosteric block of KCa2 channels by apamin. J Biol Chem. 2010 Aug 27;285(35):27067–77. doi:10.1074/jbc.M110.110072 PubMed PMID: 20562108; PubMed Central PMCID: PMC2930706.

21. Finlayson K, McLuckie J, Hern J, Aramori I, Olverman HJ, Kelly JS. Characterisation of [125I]-apamin binding sites in rat brain membranes and HEK293 cells transfected with SK channel subtypes. Neuropharmacology. 2001 Sep;41(3):341–50. doi:10.1016/S0028-3908(01)00067-3

22. Grunnet M, Jensen BS, Olesen SP, Klaerke DA. Apamin interacts with all subtypes of cloned small-conductance Ca 2+ -activated K + channels. Pflugers Arch. 2001 Jan 15;441(4):544–50. doi:10.1007/s004240000447

23. Pedarzani P, Stocker M. Molecular and cellular basis of small--and intermediate-conductance, calcium-activated potassium channel function in the brain. Cell Mol Life Sci. 2008 Oct;65(20):3196–217. doi:10.1007/s00018-008-8216-x PubMed PMID: 18597044; PubMed Central PMCID: PMC2798969.

24. Weatherall KL, Goodchild SJ, Jane DE, Marrion NV. Small conductance calcium-activated potassium channels: from structure to function. Prog Neurobiol. 2010 Jul;91(3):242–55. doi:10.1016/j.pneurobio.2010.03.002 PubMed PMID: 20359520.

25. Weatherall KL, Seutin V, Liégeois JF, Marrion NV. Crucial role of a shared extracellular loop in apamin sensitivity and maintenance of pore shape of small-conductance calcium-activated potassium (SK) channels. Proc Natl Acad Sci U S A. 2011 Nov 8;108(45):18494–9. doi:10.1073/pnas.1110724108 PubMed PMID: 22025703; PubMed Central PMCID: PMC3215033.

26. Butler AS, Hancox JC, Marrion NV. Preferential formation of human heteromeric SK2:SK3 channels limits homomeric SK channel assembly and function. J Biol Chem. 2023 Jan;299(1):102783. doi:10.1016/j.jbc.2022.102783 PubMed PMID: 36502918; PubMed Central PMCID: PMC9841042.

27. Dilly S, Philippart F, Lamy C, Poncin S, Snyders D, Seutin V, et al. The interactions of apamin and tetraethylammonium are differentially affected by single mutations in the pore mouth of small conductance calcium-activated potassium (SK) channels. Biochem Pharmacol. 2013 Feb 15;85(4):560–9. doi:10.1016/j.bcp.2012.12.015 PubMed PMID: 23270990.

28. Graulich A, Lamy C, Alleva L, Dilly S, Chavatte P, Wouters J, et al. Bis-tetrahydroisoquinoline derivatives: AG525E1, a new step in the search for non-quaternary non-peptidic small conductance Ca(2+)-activated K(+) channel blockers. Bioorg Med Chem Lett. 2008 Jun 1;18(11):3440–5. doi:10.1016/j.bmcl.2008.03.069 PubMed PMID: 18436444.

29. Ishii TM, Maylie J, Adelman JP. Determinants of apamin and d-tubocurarine block in SK potassium channels. J Biol Chem. 1997 Sep 12;272(37):23195–200. doi:10.1074/jbc.272.37.23195 PubMed PMID: 9287325.

30. Nolting A, Ferraro T, D'hoedt D, Stocker M. An amino acid outside the pore region influences apamin sensitivity in small conductance Ca2+-activated K+ channels. J Biol Chem. 2007 Feb 9;282(6):3478–86. doi:10.1074/jbc.M607213200 PubMed PMID: 17142458; PubMed Central PMCID: PMC1849974.

31. Nam YW, Im D, Garcia ASC, Tringides ML, Nguyen HM, Liu Y, et al. Cryo-EM structures of the small-conductance Ca2+-activated KCa2.2 channel. Nat Commun. 2025 Apr 17;16(1):3690. doi:10.1038/s41467-025-59061-1

32. Cassell SJ, Li W, Krautwald S, Khoshouei M, Lee YT, Hou J, et al. Mechanism of SK2 channel gating and its modulation by the bee toxin apamin and small molecules [Internet]. eLife Sciences Publications, Ltd; 2025 [cited 2025 Jul 23]. Available from: https://elifesciences.org/reviewed-preprints/107733v1 doi:10.7554/elife.107733.1

33. Ma B, Wu D, Cao E, Chi C, Wang Z, Xia Z, et al. Structural mechanisms for inhibition and activation of human small-conductance Ca2+-activated potassium channel SK2. Nat Commun. 2026 Jan 15;17(1):1770. doi:10.1038/s41467-026-68475-4

34. Katoh K, Rozewicki J, Yamada KD. MAFFT online service: multiple sequence alignment, interactive sequence choice and visualization. Brief Bioinform. 2019 Jul 19;20(4):1160–6. doi:10.1093/bib/bbx108

35. Minh BQ, Schmidt HA, Chernomor O, Schrempf D, Woodhams MD, Von Haeseler A, et al. IQ-TREE 2: New Models and Efficient Methods for Phylogenetic Inference in the Genomic Era. Teeling E, editor. Molecular Biology and Evolution. 2020 May 1;37(5):1530–4. doi:10.1093/molbev/msaa015

36. Hoang DT, Chernomor O, Von Haeseler A, Minh BQ, Vinh LS. UFBoot2: Improving the Ultrafast Bootstrap Approximation. Mol Biol Evol. 2018 Feb 1;35(2):518–22. doi:10.1093/molbev/msx281

37. Potter SC, Luciani A, Eddy SR, Park Y, Lopez R, Finn RD. HMMER web server: 2018 update. Nucleic Acids Res. 2018 Jul 2;46(W1):W200–4. doi:10.1093/nar/gky448

38. Fu L, Niu B, Zhu Z, Wu S, Li W. CD-HIT: accelerated for clustering the next-generation sequencing data. Bioinformatics. 2012 Dec 1;28(23):3150–2. doi:10.1093/bioinformatics/bts565

39. Di Franco A, Poujol R, Baurain D, Philippe H. Evaluating the usefulness of alignment filtering methods to reduce the impact of errors on evolutionary inferences. BMC Evol Biol. 2019 Dec;19(1):21. doi:10.1186/s12862-019-1350-2

40. Abramson J, Adler J, Dunger J, Evans R, Green T, Pritzel A, et al. Accurate structure prediction of biomolecular interactions with AlphaFold 3. Nature. 2024 Jun 13;630(8016):493–500. doi:10.1038/s41586-024-07487-w

41. Trott O, Olson AJ. AutoDock Vina: Improving the speed and accuracy of docking with a new scoring function, efficient optimization, and multithreading. J Comput Chem. 2010 Jan 30;31(2):455–61. doi:10.1002/jcc.21334

42. Eberhardt J, Santos-Martins D, Tillack AF, Forli S. AutoDock Vina 1.2.0: New Docking Methods, Expanded Force Field, and Python Bindings. J Chem Inf Model. 2021 Aug 23;61(8):3891–8. doi:10.1021/acs.jcim.1c00203

43. Krieger E, Vriend G. YASARA View - molecular graphics for all devices - from smartphones to workstations. Bioinformatics. 2014 Oct 15;30(20):2981–2. doi:10.1093/bioinformatics/btu426 PubMed PMID: 24996895; PubMed Central PMCID: PMC4184264.

44. Gordon JC, Myers JB, Folta T, Shoja V, Heath LS, Onufriev A. H++: a server for estimating pKas and adding missing hydrogens to macromolecules. Nucleic Acids Res. 2005 Jul 1;33(Web Server):W368–71. doi:10.1093/nar/gki464

45. Jo S, Kim T, Iyer VG, Im W. CHARMM-GUI: A web-based graphical user interface for CHARMM. J Comput Chem. 2008 Aug;29(11):1859–65. doi:10.1002/jcc.20945

46. Abraham MJ, Murtola T, Schulz R, Páll S, Smith JC, Hess B, et al. GROMACS: High performance molecular simulations through multi-level parallelism from laptops to supercomputers. SoftwareX. 2015 Sep;1–2:19–25. doi:10.1016/j.softx.2015.06.001

47. Darden TA, Pedersen LG. Molecular modeling: an experimental tool. Environ Health Perspect. 1993 Oct;101(5):410–2. doi:10.1289/ehp.93101410

48. Michaud-Agrawal N, Denning EJ, Woolf TB, Beckstein O. MDAnalysis: A toolkit for the analysis of molecular dynamics simulations. J Comput Chem. 2011 Jul 30;32(10):2319–27. doi:10.1002/jcc.21787

49. Heginbotham L, MacKinnon R. The aromatic binding site for tetraethylammonium ion on potassium channels. Neuron. 1992 Mar;8(3):483–91. doi:10.1016/0896-6273(92)90276-j PubMed PMID: 1550673.

50. Monaghan AS, Benton DCH, Bahia PK, Hosseini R, Shah YA, Haylett DG, et al. The SK3 subunit of small conductance Ca2+-activated K+ channels interacts with both SK1 and SK2 subunits in a heterologous expression system. J Biol Chem. 2004 Jan 9;279(2):1003–9. doi:10.1074/jbc.M308070200 PubMed PMID: 14559917.

51. Lenaeus MJ, Vamvouka M, Focia PJ, Gross A. Structural basis of TEA blockade in a model potassium channel. Nat Struct Mol Biol. 2005 May;12(5):454–9. doi:10.1038/nsmb929 PubMed PMID: 15852022.

52. Ahern CA, Eastwood AL, Lester HA, Dougherty DA, Horn R. A cation-pi interaction between extracellular TEA and an aromatic residue in potassium channels. J Gen Physiol. 2006 Dec;128(6):649–57. doi:10.1085/jgp.200609654 PubMed PMID: 17130518; PubMed Central PMCID: PMC2151593.

53. Goodchild SJ, Lamy C, Seutin V, Marrion NV. Inhibition of KCa2.2 and KCa2.3 channel currents by protonation of outer pore histidine residues. J Gen Physiol. 2009 Oct 1;134(4):295–308. doi:10.1085/jgp.200910252

54. Benton DCH, Garbarg M, Moss GWJ. The relationship between functional inhibition and binding for K(Ca)2 channel blockers. PLoS One. 2013;8(9):e73328. doi:10.1371/journal.pone.0073328 PubMed PMID: 24039913; PubMed Central PMCID: PMC3769273.

55. Grunnet M, Jespersen T, Angelo K, Frøkjær-Jensen C, Klaerke DA, Olesen SP, et al. Pharmacological modulation of SK3 channels. Neuropharmacology. 2001 Jun;40(7):879–87. doi:10.1016/S0028-3908(01)00028-4

56. Terstappen GC, Pula G, Carignani C, Chen MX, Roncarati R. Pharmacological characterisation of the human small conductance calcium-activated potassium channel hSK3 reveals sensitivity to tricyclic antidepressants and antipsychotic phenothiazines. Neuropharmacology. 2001 May;40(6):772–83. doi:10.1016/S0028-3908(01)00007-7

57. Fanger CM, Rauer H, Neben AL, Miller MJ, Rauer H, Wulff H, et al. Calcium-activated Potassium Channels Sustain Calcium Signaling in T Lymphocytes. Journal of Biological Chemistry. 2001 Apr;276(15):12249–56. doi:10.1074/jbc.M011342200

58. Hancock JM, Weatherall KL, Choisy SC, James AF, Hancox JC, Marrion NV. Selective activation of heteromeric SK channels contributes to action potential repolarization in mouse atrial myocytes. Heart Rhythm. 2015 May;12(5):1003–15. doi:10.1016/j.hrthm.2015.01.027

59. Sacerdot C, Louis A, Bon C, Berthelot C, Roest Crollius H. Chromosome evolution at the origin of the ancestral vertebrate genome. Genome Biol. 2018 Dec;19(1):166. doi:10.1186/s13059-018-1559-1

60. Ohno S. Evolution by Gene Duplication. Springer Berlin Heidelberg. 1970.

61. Holland LZ, Ocampo Daza D. A new look at an old question: when did the second whole genome duplication occur in vertebrate evolution? Genome Biol. 2018 Dec;19(1):209. doi:10.1186/s13059-018-1592-0

62. Marlétaz F, Timoshevskaya N, Timoshevskiy VA, Parey E, Simakov O, Gavriouchkina D, et al. The hagfish genome and the evolution of vertebrates. Nature. 2024 Mar 28;627(8005):811–20. doi:10.1038/s41586-024-07070-3

63. Kuraku S. Impact of asymmetric gene repertoire between cyclostomes and gnathostomes. Semin Cell Dev Biol. 2013 Feb;24(2):119–27. doi:10.1016/j.semcdb.2012.12.009

64. Tan M, Redmond AK, Dooley H, Nozu R, Sato K, Kuraku S, et al. The whale shark genome reveals patterns of vertebrate gene family evolution. eLife. 2021 Aug 19;10:e65394. doi:10.7554/eLife.65394

65. Inoue J, Sato Y, Sinclair R, Tsukamoto K, Nishida M. Rapid genome reshaping by multiple-gene loss after whole-genome duplication in teleost fish suggested by mathematical modeling. Proc Natl Acad Sci USA. 2015 Dec;112(48):14918–23. doi:10.1073/pnas.1507669112

66. Qi M, Clark J, Moody ERR, Pisani D, Donoghue PCJ. Molecular Dating of the Teleost Whole Genome Duplication (3R) Is Compatible With the Expectations of Delayed Rediploidization. Van De Peer Y, editor. Genome Biology and Evolution. 2024 Jul 3;16(7):evae128. doi:10.1093/gbe/evae128